Dust observations with antenna measurements and its prospects for observations with Parker Solar Probe and Solar Orbiter

Ingrid Mann[1], Libor Nouzák[2], Jakub Vaverka[2], Tarjei Antonsen[1], Åshild Fredriksen[1], Karine Issautier[3], David Malaspina[4], Nicole Meyer-Vernet[3], Jiří Pavlů[2], Zoltan Sternovsky[4], Joan Stude[5], Shengyi Ye[6], Arnaud Zaslavsky[3]

[1]Department of Physics and Technology, UiT The Arctic University of Norway, 9037, Tromsø, Norway
[2]Department of Surface and Plasma Science, Charles University, Prague, 180 00, Czech Republic
[3]LESIA - Observatoire de Paris, Université PSL, CNRS, Sorbonne Université, Université de Paris, 5 place Jules Janssen, 92195 Meudon, France
[4]Laboratory for Atmospheric and Space Physics, University of Colorado, Boulder, CO 80303, USA
[5]Deutsches Zentrum für Luft- und Raumfahrt, Institut für Physik der Atmosphäre, Oberpfaffenhofen, Germany
[6]Department of Physics and Astronomy, University of Iowa, Iowa city, 52242-1479, Iowa, USA
Correspondence to: Ingrid Mann (ingrid.b.mann@uit.no)

Abstract. The electric and magnetic field instrument suite FIELDS on board the NASA Parker Solar Probe and the radio and plasma waves instrument RPWS on the ESA Solar Orbiter mission that explore the inner heliosphere are sensitive to signals generated by dust impacts. Dust impacts were observed using electric field antennas on spacecraft since the 1980s and the method was recently used with a number of space missions to derive dust fluxes. Here, we consider the details of dust impacts, subsequent development of the impact generated plasma and how it produces the measured signals. We describe empirical approaches to characterise the signals and compare to a qualitative discussion of laboratory simulations to predict signal shapes for spacecraft measurements in the inner solar system. While the amount of charge production from a dust impact will be higher near the sun than observed in the interplanetary medium before, the amplitude of pulses is determined by the recovery behaviour that is different near the Sun since it varies with the plasma environment.

1 Introduction

The space missions Parker Solar Probe and Solar Orbiter to explore the inner heliosphere and close vicinity of the Sun carry antennas experiments that respond to dust impacts onto the spacecraft. Parker Solar Probe (Parker Probe) is a NASA mission that was launched in August 2018 and that studies the vicinity of the Sun at closest distance ~ 10 solar radii near the solar equator. The mission payload includes the electric and magnetic fields instrument suite FIELDS (Bale et al. 2016). Solar Orbiter is an ESA mission with a launch planned in 2020 (Mueller and al., 2019). It will study the vicinity of the Sun as close as 0.3 AU and at maximum 35° inclination from the Solar equatorial plane includes the Radio and Plasma Waves (RPW) experiment (Maksimovic et al., 2019). Dust impacts are

observed with electric antennas for field measurements since the 1980s beginning with the Voyager mission (cf. Gurnett et al., 1997, Meyer-Vernet, 2001). The method was recently used with a number of space missions to derive dust fluxes. While antenna measurements do not replace those of dedicated dust detectors, they are interesting

35 because many space missions carry electric field instruments ~~than carry dedicated dust detectors~~. In addition, antenna measurements can observe lower dust fluxes because of their large collecting area of the whole spacecraft in comparison to the small collecting area of dust detectors. A limitation of the antenna measurements is that they do not provide information on dust composition and only limited information, if at all, on impact direction and dust mass. These derived values are highly uncertain (Meyer-Vernet et al. 2009, Zaslavski et al. 2012, Malaspina et al.

40 2015). The relationship between dust impacts and the signals they produce in electric field instruments has also been considered in new instrument development and laboratory measurements.

Cosmic dust particles are one of the major constituents of the interplanetary medium in the inner heliosphere and knowledge on dust near the Sun is so far based on remote observations and model assumptions. An exception are

45 the measurements of the HELIOS mission with two spacecraft that reached a minimum distance 0.31 AU from the Sun and each carried a dust detector (Grün et al. 1980). Our basic understanding (see, e.g. Mann et al. 2004) is that large (> micrometre) dust particles that are fragments of comets and asteroids are in Keplerian orbits around the Sun. Their velocities and number densities increase with decreasing distance from the Sun. Fragments are produced in dust-dust collisions for which the rates increase with decreasing distance from the Sun. The majority of fragments

50 smaller than micrometre are pushed outward by radiation pressure (cf. Wehry and Mann 1999) and deflected by electro-magnetic forces (cf. Mann et al. 2004, Czechowski and Mann 2010). In addition to the interplanetary dust, interstellar dust particles stream into the inner heliosphere from interstellar upstream direction and move ~parallel to the ecliptic plane (Mann 2010). Because of repulsion by the radiation pressure force, only the large interstellar dust reaches the inner heliosphere. A large fraction of dust is destroyed in the inner heliosphere, in sublimation and

55 other destruction processes and this generates a dust-free zone. Sun-grazing comets (cf. Jones et al. 2018) are a local highly variable source for dust particles (cf. Fig. 1). Dust material is released in the ambient solar wind, a process which is not well quantified. The solid fragments that are not fully destroyed are pushed outward and produce the small size portion of the interplanetary dust flux observed near Earth orbit. Parker Probe and Solar Orbiter will for the first time explore the inner heliosphere in-situ. The dust impacts on the spacecraft will influence

60 electric field measurements on these spacecraft and provide an opportunity to study the dust environments of the inner heliosphere.

This paper discusses dust detection with electric field measurements based on recent observations from several spacecraft, and it discusses the prospects of studying dust impacts with the two space missions to the inner heliosphere. We start by describing the impact ionisation of dust particles (section 2), followed by a qualitative discussion of the dust impact signal generation in the vicinity of the spacecraft (section 3) and resulting antenna signal shapes (section 4). Section 5 discusses the signals and observations made recently with other space missions. In section 6 we describe our current state of knowledge on dust in the inner heliosphere and in section 7 we discuss implications for observations with Parker Probe and Solar Orbiter.

2 Dust Impact Ionisation

Dust impacts on the spacecraft body generate clouds of ions and electrons through a process known as impact ionisation. An impact ionisation model suggested by Drapatz and Michel (1974) can be summarised as follows: Dust grains impacting onto the spacecraft at speeds that are supersonic in the target solid, i.e. faster than the order of a few kilometres per second, produce a shock compression waves in the solid which shatters, vaporises and ionises the dust as well as material of the target where an impact crater forms. Free charges in the form of electrons and atomic and molecular ions are produced by thermal ionisation of the impact vapour. The initial ionisation is followed by recombination and thermalisation and a residual ionisation remains in the impact vapour. The amount of the residual ionisation can be derived from laboratory measurements of the charge production. An empirical relation describes the charge production Q, as a function of the dust mass, m and speed, v according to $Q = \xi m^\alpha v^\beta$, where Q is given in Coulombs, the m in kilograms and v in km/s. The exponents α and β are dimensionless and determined from experimental data. The constant ξ gives the proportionality and, as parameters α and β, it is dependent on both impactor and target composition. This impact ionisation model (cf. Drapatz and Michel, 1974) is in a good agreement with laboratory experiments in relatively thin targets, for speeds between the supersonic limit and some tens of km/s. The model bases on the assumption that neutral vapour forms in the impact process and that it subsequently ionises because of its high temperature. Ionisation can also occur directly in the target where the propagating shock wave leads to a high-pressure high temperature state so that the ejected target material is already ionized (see Hornung and Kissel 1994). The properties of the vapour cloud are also depending on material composition and on the impact angle (cf. Sugita et al. 1998). Moreover, the shock wave propagation in the target (spacecraft) and dust material produces not only vapour, but also solid fragments and the fragment formation is predominant at smaller impact velocities (Jones et al. 1996). In summary, there is no theory that fully describes the charge production, sometimes also denoted as plasma production, that is caused by dust impacts onto

spacecraft. The following discussion uses the term impact cloud for the impact generated electrons, ions, and neutrals to avoid confusion with the surrounding plasma.

95 Charge production is often determined empirically in dust accelerator facilities, in recent years at those of the University of Stuttgart (Mocker et al., 2011) and the University of Colorado (Shu et al., 2012) for the range of impact velocities shown in Figure 2. The parameters to describe impact charge production derived from observations vary strongly for different impact materials; α has reported values between 0.7 and 1 while β has been measured between 2.5 and 6.2 (see e.g. Dietzel et al. 1973, Auer 2001, Collette et al. 2014, and references therein).

100 An often-used relationship for dust impacts on spacecraft is $Q \approx 0.7mv^{3.5}$, which was reported for aluminium targets (McBride and McDonnell, 1999). It should be noted that the exponents also change for low impact energies (speeds below ~1 km/s and sizes below ~10 nm). For low energy collisions, where fragments of significant sizes compared to the initial impactor survive, there may be surface effects such as capacitive contact charging (see e.g. John et al. 1980). The exponent also changes at high impact energies for speeds above ~50 km/s and dust sizes

105 above ~1 μm (Auer 2001; Göller and Grün, 1989). Collette et al. (2014) measured the charge impact yield as a function of impact velocity for common materials used on spacecraft, they point out the need for dedicated studies for > 50 km/s impacts. For very large impact energies, where the impactor gets completely vaporised, surface effects are negligible and the charge generation can be modelled through hydrodynamic theory (Hornung and Kissel, 1994). Moreover, there is a dependence of impact angle on the charge generation (Schulz and Sugita, 2006;

110 Collette et al. 2014). Based on spectroscopic analysis of 4.7 – 5.6 km/s impact flashes Sugita et al. (1998) find temperatures of about 4000 K to 5000 K for the impact vapour cloud. Subsequent observations yield temperatures of 0.9 to 3 eV for impact speeds varying from 10 to 40 km/s (Miyachi et al. 2008). Laboratory measurements find for the impact vapour ion temperatures of about 5 eV at 4 km/s impact speed and > 10 eV at 20 km/s (Collette et al. 2016).

115 **3 The Impact Process**

Formation of the dust impact signal involves the dust impact process, the interaction of the impact cloud with the surrounding plasma and finally the detection by electric field measurement. At the most basic level, dust impacts on the spacecraft body generate clouds of free electrons and positive or negative ions. These charged particles are attracted to, or repulsed from, the spacecraft surface according to its electric potential relative to the surrounding

120 ambient plasma. Charged particles from the impact cloud can be re-collected by the spacecraft or escape to free

space and generate a transient deviation from the equilibrium spacecraft surface potential. The potential change can be positive or negative, e.g., escaping electrons generate a positive signal. Electrons are significantly faster than ions, thus the signal generated by escaping electrons appears before the signal generated by escaping ions for the case when the spacecraft potential is not too large. The amplitude of the spacecraft potential deviation is given by the amount of escaped charges and by spacecraft capacitance. The spacecraft potential relaxes back to the equilibrium value via interaction with ambient plasma according to $\Phi_{SC} \sim e^{-t/\tau}$, where τ *is* a characteristic relaxation time (Meyer-Vernet, 1985).

The different phases of the impact process for various spacecraft potentials (slightly positive, zero, and slightly negative) are illustrated in Fig. 3. In the first phase (T1), at which the spacecraft is assumed to be in equilibrium potential, the impact occurs, and an impact cloud is generated (green). Some of the cloud particles may be re-collected. The second phase (T2) is characterised by electron escape and partial recollection depending on the target's potential, yielding an initial rise in signal strength (blue). The third phase (T3) is characterised by the ion escape, decreasing the spacecraft potential (red). The final phase (T4) is the relaxation phase when the spacecraft potential returns to the equilibrium value (orange). Individual time steps are summarised in Table 1 and sketched in Fig. 3. The ratio between escaping electrons and ions in phases T2 and T3 depend on the spacecraft potential. For example, more electrons than ions leave for a negatively charged spacecraft (left part of Fig. 3).

3.1 Impact cloud generation and expansion - T1

Charged particles at a small distance from the spacecraft body still influence its potential. The change in the spacecraft potential can thus not be observed directly after impact cloud formation but when charged particles are recollected or escape far enough and/or are sufficiently shielded by the ambient plasma or photoelectrons that their influence on the spacecraft potential is reduced (Meyer-Vernet et al. 2017). The number of escaping particles depends on initial impactor energy and velocity after the initial cloud expansion. It is possible to assume that impact cloud electrons move in random directions due to collisions with ions. This implies that half of the electrons move towards the spacecraft before they are influenced by spacecraft potential, whereas the other half moving initially outwards is recollected if the target potential is positive and higher than their temperature (in eV). An alternative model assumes approximately half of both the electrons and the ions move towards the spacecraft. This model is in good agreement with recent laboratory measurements (Nouzák et al., 2018, see below). It bases on the

assumption that the impact vapour is initially neutral and that the free charges form as a result of thermal ionisation in the impact vapour.

3.2 Electron escape - T2

The first part of the signal shown in Fig. 3 is generated by electrons escaping from the spacecraft body. The amplitude of the electron signal is reduced when the spacecraft is charged positively because some electrons are attracted back to the spacecraft. All electrons are re-collected when the positive spacecraft potential is significantly higher than the temperature of electrons (no electron part in the signal). This is a very fast process (µs) and the characteristic time depends on a number of parameters. Independent from the ambient plasma this process is influenced by the geometry of the system and specifics of the antenna and parts of the spacecraft body as well as the energy (velocity) of the electrons. The cloud expansion and internal shielding depends on the size of cloud formed by the impact. In space, the ambient plasma Debye length and magnitude of the photoemission current from the spacecraft determine the length scale of the spacecraft potential influence on the expansion.

3.3 Ion escape - T3

The ion escape works in a similar manner as electron escape, but happens at a lower rate if electron and ion temperature are comparable. The potential induced by ions on the spacecraft and antennas is progressively shielded by the ambient plasma electrons and photoelectrons. Moreover, escaping electrons can drag some of the ions behind them. This can result in double population of escaping ions: fast and slow. All ions are recollected when the negative spacecraft potential is significantly higher than the temperature of ions.

3.4 Relaxation - T4

The spacecraft potential returns back to the equilibrium value due to interaction with ambient plasma. The relaxation time is determined by the ambient environment (plasma density, temperature, photoemission), and by the capacitance of the spacecraft and antennas. On the other hand, higher plasma density and stronger photoemission result in stronger currents from ambient plasma and thus in a significantly shorter relaxation time. The typical relaxation time measured by various spacecraft is in the range from $\approx$ 100 µs up to several ms. The relaxation time could be comparable or shorter than the ion escape or shielding time in dense plasma environments (or under strong photoemission), and by the capacitance of the spacecraft and antennas. This will result in a reduction of the detected signal and lowers the sensitivity of dust detection via electric field antennas. Relaxation

time can also be reduced by active experiments, for example by ASPOC (Active Spacecraft POtential Control) (Vaverka et al., 2017b).

4 Antenna Signal Shapes

Electric field antennas can be operated as a dipole, where the voltage difference between two antenna booms is measured, or a monopole, where the voltage difference between an antenna boom and the spacecraft body is measured. It has been noted that the power spectral density of dust impact signals measured by monopole antenna is significantly larger than that measured by the dipole antennas (Meyer-Vernet 1985, Tsintikidis et al., 1994; Meyer-Vernet et al., 2014), and this difference is attributed to the low sensitivity of a symmetric dipole antenna to dust impacts on spacecraft body. It is important to note that dust impact on a spacecraft body described by this model, can be detected by the monopole electric field antenna as a potential drop between the spacecraft body and one antenna. A dipole configuration measuring electric field as a potential difference between two antennas can be utilized to detect a signal only when escaping electrons or ions influence the potential of one of the dipole antennas asymmetrically. The described model shows a strong dependence on the spacecraft potential. This can be compared with laboratory experiments for various polarity and sizes of bias voltage. A series of such measurement campaigns have been performed at the dust accelerator facility at the University of Colorado in order to aid the interpretation of signals collected in space. Collette et al. (2015) successfully identified different mechanisms of voltage signals generation on the antennas. The experiments performed by Nouzák et al. (2018) have used a scale model of the Cassini spacecraft to investigate the differences between antennas operated in monopole vs. dipole modes. The results show that in the dipole mode the antennas are greatly insensitive to dust impacts occurring on the spacecraft and only impacts on the antennas generate clear signals. This study helped clarifying the appropriate cross section to be used for calculating the density of dust populations encountered by the spacecraft (Ye et al., 2016).

A few cases of impact events are shown in Fig. 4 derived from laboratory studies on scaled down Cassini model (Nouzák et al., 2018). Although the signals are measured in dipole configuration, since the dust impacts one of the dipole antennas, this configuration corresponds to monopole measurement when dust impacts the spacecraft body as described above. The laboratory experiment is performed in the vacuum chamber without ambient plasma. Relaxation process is simulated by discharge of electronics circuit inside of the Cassini model.

205 Figure 4 shows different signal shapes measured in the Cassini laboratory simulation and the signal development of the different stages are described for each case in Table 2:

- The signal shown in panel (A) is for a strongly negatively biased target potential. All electrons are repulsed from the spacecraft and all ions are recollected back to a strongly negatively biased target. The ion escape part (red) is not apparent in this case. The electron part (blue) is followed directly by
210   relaxation (orange).

- Panel (B) describes the signal shape for a reduced negative target potential. The number of escaping ions increases with the reduction of the negative potential (panel B). The electron part (blue) is followed by the smaller ion part (red) and relaxation (orange). A kink appears between the ion part (red) and relaxation (orange) see a left panel in Fig. 3.

215 - Panel (C) describing the signal measured at an unbiased target shows that similar numbers of electrons and ions escape. The amplitude of the electron part (blue) is similar to the ion part (red).

- Panel (D) shows the case of positively charged target. The number of escaping electrons is reduced and the ion part of the signal exceeds the electron one. This results in a bipolar signal where the first part is typically called "pre-spike" (Collette et al. 2015, Thayer et al. 2016). A larger number of escaping ions
220   change the polarity of the signal.

- Panel (DD) shows the signal for a higher positive target bias potential- The first (electron) part of the bipolar pulse is reduced with increasing positive target potential.

- Panel (E) shows a case of even higher positive bias. All electrons are re-collected in this case. The signal has no electron (blue) part and it has no "pre-spikes" in this case.

225

The shapes of all pulses measured in the laboratory for various biases can be explained by the model described above. It must be noted, however, that since electron and ion escapes are very fast processes (~µs), detection of a detailed structure of initial parts of pulses including "pre-spikes" thus requires fast electronics (sampling in the order of 100 kHz). Therefore, not all spacecraft are able to detect them, and a thorough inquiry into signal shapes

230 using in-situ data is difficult. . The antenna signal can be also affected by the response of instrument electronics. For example, transfer function of electronics can modify a shape and duration of the measured signal (Ye et al., 2019).

5 Antenna signals observed in previous space missions

235 Detection of dust impacts with antenna measurements has recently been done in several space missions. In the following, we discuss the major findings related to dust detection from the respective missions.

5.1 STEREO

STEREO is a NASA mission that was launched on October 26, 2006, with the study of coronal mass ejections as primary science goal. The mission consists of two twin spacecraft that orbit the Sun at around 1 AU, one trailing
240 the Earth (STEREO B) while the other leads (STEREO A). The study of the STEREO/WAVES radio receiver data proved to be of great interest for dust studies. STEREO/WAVES measured the flux of sub- micrometre dust near 1 AU (Meyer-Vernet et al. 2009, Belheouane et al. 2012, Zaslavsky et al. 2012) and discovered a highly time-variable flux of dust with size few nm (Meyer-Vernet et al., 2009). The nanodust impacts were observed frequently on both STEREO spacecraft as radio pulses on single monopole antennas. The physical mechanism that leads to their
245 generation is not yet fully understood. The voltage was much higher on the antenna that was adequately located to be sensitive to impacts of prograde nanodust on each spacecraft (Meyer-Vernet et al. 2009), which destabilized the photoelectron sheath of that antenna (Pantellini et al., 2012), producing a ratio between antenna voltages in agreement with the mechanism producing the pulses (Zaslavsky et al. 2012). The formation of the signal involves a transient local perturbation of the photoelectron equilibrium current on the antenna being close to the impact. The
250 steps that lead to the antenna signals have been studied with plasma simulations and semi-empirically (see e.g. Pantellini et al., 2012; Meyer-Vernet et al., 2014; Zaslavsky, 2015). Kellogg et al. 2018 suggested that STEREO does not observe nanodust, but did not propose an alternative mechanism able to explain the observations. The larger dust impacts observed with STEREO/WAVES are observed with similar amplitudes at all three antennas. Based on STEREO/WAVES Zaslavsky (2015) proposed a model accounting for electric pulses generation by
255 electron collection after an impact, linking the shape and amplitude of the electric signals to the dust and local plasma parameters. Figure 5 shows the model applied to typical impact clouds.

5.2 Cluster

The Cluster mission launched in 2000 consists of four identical spacecraft orbiting the Earth in close formation. The highly elliptical orbit (4–20 Earth radii) crosses various parts of the Earth's magnetosphere. Each spacecraft is
260 equipped with two pairs of dipole electric field sensors (on 88 m booms tip-to-tip) (Gustafsson et al., 2001). Wide Band Data (WBD) instrument provide data of single electric or magnetic field component with a high sampling

frequency in three modes (27.4 kHz, 54.9 kHz, and 219.5 kHz) (Gurnett et al., 1997). This resolution is sufficient to detect signals triggered by dust impacts. The dipole configuration is not sensitive to dust impacts on the spacecraft body. Some signal can be detected only after a direct dust impact on the one of the antennas or when the expanding impact cloud influences the potential of the antenna. On the other hand, Cluster 1 operates with the only one remaining probe in the monopole configuration since 2009 (three probes have been lost during time). This situation makes the detection of dust impacts by the Cluster 1 spacecraft possible (Vaverka et al., 2017a). On the other hand, a presence of a large number of natural waves including electrostatic solitary waves in the Earth's magnetosphere significantly complicates such detection (Vaverka et al., 2018). The fact that solitary waves are much more numerous than the expected amount of detected dust grains makes a reliable detection of dust impacts by the Cluster spacecraft very challenging. For this reason, the Cluster spacecraft are not optimal for dust studies.

5.3 MMS

The MMS mission consists of four Earth-orbiting spacecraft lunched in 2015 (Burch et al., 2016). While the missions are similar, the MMS electric field instruments just slightly differ from the Cluster ones. Each of the spacecraft is equipped with three pairs of electric field probes, two in the spin plane (120 m tip-to-tip) and one in the axial plane (29 m, Torbert et al., 2016). The electric field is measured in the dipole configuration in all three directions with sampling frequency up to 8 kHz (burst mode) and up to 256 kHz in wave burst mode. The main difference is that the instrument operates simultaneously also in the monopole configuration. The combination of dipole and monopole measurements provides a complex information about the ambient electric field and the spacecraft potential which is possible to use for the reliable identification of dust impacts. Solitary waves and other structures in the ambient plasma or electric field generate simultaneously pulses both in monopole and dipole configuration. On the other hand, changes in the spacecraft potential triggered by the dust impact generate identical pulses on all monopole antennas and no signal in the dipole configuration (electric field data). This allows us reliably distinguish changes in the spacecraft potential from the other pulses as solitary waves (see Vaverka et al., 2018). A measurement with MMS, shown in Fig. 6, illustrates the different detections in monopole and dipole configuration.

5.4 Maven

MAVEN is a NASA mission to Mars. It launched on November 18, 2013 and arrived at Mars on September 22, 2014. MAVEN is designed to study the escape of Mars's atmosphere, including the contribution of plasma

processes associated with the interaction between the solar wind and the planet (Jakosky et al. 2015). Voltage spikes consistent with the impact of micron dust on the spacecraft were detected by the MAVEN LPW (Langmuir Probe and Waves) experiment at orbital altitudes between 200 km and 1500 km (Andersson et al. 2015a). Andrews et al. 2015 found large variations in plasma density and spacecraft surface charging encountered by MAVEN as it dipped into the Martian ionosphere. This resulted in strong variation in the detectability of dust impact voltage spikes. Once these effects were taken into consideration, the estimated near-Mars micron dust flux observed by MAVEN was found to be consistent with the interplanetary dust flux expected at Mars (Andersson et al. 2015b). No evidence for moon-related dust rings or dust lifted from the surface (e.g. Sanchez-Lavega et al. 2015) was found with MAVEN LPW.

5.5 Wind

The NASA Wind spacecraft launched in November 1994 with the goal of studying the solar wind upstream of Earth. From 1994 to 2004, Wind executed a series of high apogee (100 R_e) orbits about Earth and several lunar flybys before being stationed in an orbit about the first Lagrange point (L_1) ~250 Re Sunward of Earth, where it remains operational to the present day (2019). The Wind WAVES experiment (Bougeret et al. 1995) detects voltage spikes consistent with the impact of micron-sized dust on the spacecraft body (Malaspina et al. 2014). These dust spikes are observable even though Wind WAVES makes only dipole electric field measurements, likely due to strong asymmetries of the dust impact signal on oppositely mounted antennas. Further, the rapid spin of the Wind spacecraft (one rotation every 3s) and asymmetry of dust impact voltage signals on the electric field wire antennas allows a crude directionality of the dust to be determined (Malaspina et al. 2014, Malaspina and Wilson 2016). The observed amplitude and polarity of such signals are consistent with voltage induced on the antennas by positive ions produced by impacts on the spacecraft, after it has recollected the electrons (Meyer-Vernet et al. 2014); this new mechanism explained the previously unexplained voltage sign and amplitude for interstellar dust impacts on Wind, and also the absence of nanodust detection on this spacecraft. The yearly modulation of Wind-observed impacts was found to be consistent with the yearly variation in interplanetary micron dust (Malaspina et al. 2014, Wood et al. 2015). Further supporting this conclusion was the observation that both Wind and STEREO observe the same yearly modulation of interstellar dust flux (Kellogg et al. 2016). The long duration of the Wind mission (> 25 years, over two full solar cycles) presents a unique opportunity to study how the solar magnetic field modulates the entry of interstellar dust into the solar system and its arrival at 1 AU. To facilitate such studies, a database cataloguing all dust impacts observed by Wind was created (Malaspina and Wilson 2016) and made

320   publicly available through the NASA Space Physics Data Facility Coordinated Data Analysis Web (CDAWeb) (https://cdaweb.sci.gsfc.nasa.gov/index.html/).

5.6 Cassini

The Cassini Radio and Plasma Wave Science (RPWS) instrument measures oscillating electric fields over the frequency range 1 Hz to 16 MHz and magnetic fields in the range 1 Hz to 12 kHz (Gurnett et al., 2004). The
325   instrument uses three nearly orthogonal electric field antennas (E_u, E_v, E_w, each 10 m long and 2.86 cm in diameter) and three orthogonal magnetic search coil antennas. The E_u and E_v antennas are often used together as a dipole antenna and E_w and the spacecraft body as a monopole antenna (Gurnett, 1998), both sensitive to dust impacts. The south-polar plume of Enceladus was one of the top discoveries made Cassini mission. During the Enceladus plume crossing, besides dust impact signals, RPWS detected plasma oscillations induced by dust impacts, the frequencies
330   of which are equal to the local plasma frequencies (Ye et al. 2014a), which can be explained by a beam-plasma instability induced by the impact-produced electrons when their speed exceeds the thermal speed of the ambient plasma (Meyer-Vernet et al. 2017). Comparison of observations (Ye et al., 2014b), showed that the dust density profile measured by RPWS is consistent with that measured by the dedicated dust detector on board.

335   Cassini allowed for a comparison of measurements in dipole and monopole configuration. The difference is clearly seen on Fig. 7 which shows the electric power spectrum measured by the Cassini Radio and Plasma Wave Science (RPWS) HFR receiver simultaneously in dipole (top) and monopole (bottom) mode in Saturn's E-ring at the first close approach of Enceladus (Meyer-Vernet et al. 2014). During the subsequent mission, the Wideband receiver (WBR) of the RPWS instrument was switched from monopole mode to dipole mode at a ring plane crossing, so
340   that the responses of these two antenna modes to dust impacts were compared, assuming the dust density and size distribution did not change across the ring plane (Ye et al., 2016). Figure 8 shows an RPWS wave power spectrogram, which covers a one-hour period around a ring plane crossing on DOY 001, 2016. As the antenna mode switched from monopole to dipole at the ring plane at ~10:30, the spectral power decrease was accompanied by a significant decrease in the negative impact rates (blue) and the polarity ratio jumping to ~1. The spectral power
345   is proportional to the product of impact rate and average voltage jump size squared (Meyer-Vernet, 1985). So, the difference in spectral power at the antenna switch could be due to either lower impact rate or smaller average voltage pulse size, or both.

In figure 9, we show a comparison of the vertical dust density profiles measured by RPWS Wideband Receiver (WBR) and the Cassini Dust Analyzer (CDA) High Rate Detector (HRD) during the ring plane crossing on DOY 361, 2016. HRD uses polarized foils for dust detection and can measure high impact rates of particles bigger than a size threshold that depends on the impact speed (Srama et al.,2004). Discontinuities in the RPWS dust density profile are due to gain changes of WBR. The CDA data showed consistent peak densities around 0.04 m^{-3} (threshold ~ 0.8 micron) during the Ring Grazing orbits, less than one order of magnitude higher than the RPWS dust density, which is within the uncertainty limit of the method (Ye et al., 2014). The density peak measured by RPWS (FWHM 600 to 1000 km) is wider than that by CDA (averaged profile shows a FWHM of 475 km). This difference is discussed in detail in Ye et al. (2018a). The E ring density structure based on RPWS measurements has been shown to be consistent as well with that revealed by optical observation (Ye et al., 2016a).

Ye et al. (2016b) compared the data collected with these two antenna setups and found that the wave power spectral density observed by the monopole antenna is ≈ 10 dB higher than that observed by the dipole antenna. This does not necessarily mean that the monopole antenna is more sensitive to individual dust impacts, because direct comparison of the waveforms observed by these two antennas showed that the sizes of the voltage jumps induced by dust impacts are comparable. Comparison of the impact rates showed that the monopole antenna detects ≈ 10 times more dust impacts than the dipole antenna. This difference in impact rates is roughly in line with the difference in the effective impact areas of the spacecraft body and the dipole electric antenna. Detailed analysis showed that the polarity ratio of the impacts detected by the dipole antenna changes with the projected area ratio of the dipole antenna elements (E_u and E_v) as the spacecraft rotates, providing strong evidence that the dipole mode detects primarily impacts on the antenna booms.

Cassini cruise measurements between 1 and 5 AU also enabled us to study the rise time of the impact ionisation pulses as a function of dust mass and of heliocentric distance (Meyer-Vernet et al. 2017), a quantity of great importance for future missions since it determines the frequency range and voltage amplitude for dust detection.

6 Dust in the inner heliosphere

Many dust observations describe the dust flux near Earth orbit, it can be estimated from meteor observations, crater statistics and measurements from spacecraft. Based on these sources, an empirical polynomial mass distribution

was found (Grün et al., 1985; Ceplecha et al., 1998). Observations by the STEREO spacecraft allowed extending this distribution to smaller masses (Zaslavsky et al., 2012, Meyer-Vernet et al., 2009, Malaspina et al. 2015). There is still an uncertainty, however on the absolute flux values. Estimates of cosmic dust fluxes near 1 AU and onto Earth range over several orders of magnitude and are based on a number of different assumptions (cf. e.g. Nesvorný et al. 2011, Mann et al., 2011; Plane, 2012). There is even less known on the dust flux inside 1 AU and estimates are often based on extrapolation of the flux curve obtained near Earth and considering the major forces acting on dust particles (Mann et al. 2004): Large dust particles ("micron dust" $m > 10^{-14}$ kg) are mainly influenced by gravity force and move in Keplerian orbits superimposed by a slow migration inward caused by the Poynting-Robertson effect. For dust with masses 10^{-19} kg $< m < 10^{-14}$ kg ("beta meteoroids") the radiation pressure force is comparable to the gravitation; when these small particles form, typically by collisions of larger dust, they move outward in hyperbolic orbits (Czechowski and Mann 2007). For even smaller dust with $m < 10^{-19}$ kg (nanodust) electromagnetic forces prevail, they are deflected in a way that is similar to the pick-up process of ions that newly form in the solar wind (Mann et al., 2010).

The observational studies of scattered light and thermal emission from the dust are constrained by large contributions from dust near Earth to the brightness because the observed brightness is an integrated signal along the line of sight (Mann et al., 2004). Since early infrared eclipse observations (MacQueen, 1968) showed irregularities in the slope of the corona brightness with varying distance from the solar limb, the possibility of dust rings existing around the Sun is discussed. Indeed, model calculations were made to show that dust rings can form for specific dust properties in the initial stage of dust sublimation when the dust size is reduced and the radiation pressure force increases with reduced dust size (Mukai and Yamamoto, 1979). The solar eclipse observations made over the years suggest however that the observed features can be explained without the existence of pronounced rings (Mann 1992) and that the average dust properties in the inner heliosphere change over time scales of years (Kimura et al., 1997; Ohgaito et al., 2002). The spatial distribution of the dust that can be derived from the scattered light and thermal emission observations suggests that the dust number density increases with distance from the Sun and in combination with the increasing orbital velocities this leads to increasing dust flux inversely proportional to the distance, r from the Sun within or close to the ecliptic plane (Mann et al. 2004). The amount of dust above the solar poles and in orbits with high inclination is even less known (Mann et al. 2004). Recent white light observations from STEREO A (Stenborg and Howard 2017a, 2017b) provide the shape of the F-corona and inner Zodiacal light from 5 to 24 degree line-of-sight elongation and show its flattening to larger elongation. Closer analysis also showed that the flattening varied with spacecraft position indicating an influence of the dust brightness near the

spacecraft (Stenborg, et al.2018, Stauffer et al. 2018), again showing the importance of considering the line-of sight
410   effects when analysing brightness observations.

While we can expect that the flux of large particles in the inner solar system increases proportional to 1/r, where r ist the distance from the Sun, it is difficult to predict the flux of smaller dust. Detailed trajectory calculations show that nanodust can be trapped in orbits with perihelia very close to the Sun instead of being ejected (Czechowski
415   and Mann, 2010). Trapping conditions depend on a number of different parameters so that the nanodust flux outward can vary in time (Czechowski and Mann, 2010, 2012). The majority of nanoparticles and those that form at distances 0.2 AU from the Sun or larger are usually ejected outward. Figure 10 shows the velocity of nanoparticles that are ejected from circular orbit at 0.2 AU. While the particles gradually gain speed, one can see that in the inner solar system they still have a velocity close to that of the parent object. The trajectory of the largest
420   particle shown in the figure with approximate radius 100 nm corresponds to a beta-meteoroid that is mainly influenced by radiation pressure force (Wehry and Mann, 1999) because it has a smaller value of surface charge to mass than the smaller particles. Figure 11 shows the velocity as function of distance for the same range of parameters for the nanodust but when particles are released from initially highly elongated orbits. The orbital eccentricity and perihelion assumed for the model calculations presented correspond to the orbits of the Aquarids
425   meteoroids and the nanoparticles are released at different locations of the orbit. One can see that their trajectories in the inner solar system strongly depend on the initial condition.

In addition to uncertainty of the dust trajectories, the dust production rate is hard to predict. The majority of dust smaller micron-size inside 1 AU are produced by fragmentation during collisions of larger dust. The dust formation
430   by mutual collisions depends on the dust material compositions (Ishimoto and Mann, 1999; Mann and Czechowski, 2005), it varies with the dust velocities and it is for instance enhanced when coronal mass ejections push out nanoparticles (Czechowski and Kleimann 2017). Sun grazing comets (cf. Jones et al. 2018) are another source of time variable dust flux. The nanodust flux can vary also due to other effects, like the variation of the source, e.g. when the dust flux is enhanced by a single collision event in the inner heliosphere, or due to the influence of the
435   solar magnetic field structure (see Czechowski and Mann 2012, Juhasz and Horanyi, 2013). While estimates are made for time-stationary conditions, current sheet crossings occur along the trajectories and in addition, the magnetic field is time-variable. Also coronal mass ejections change the conditions pushing outward large fractions of nanodust and with speed reaching 1000km/s (Czechowski and Kleimann 2017).

From ten years of STEREO A observations attributed to nanodust impacts several important properties can be obtained. The signal explained as nanodust is 10-100 times more frequent during Stream Interaction Region (SIR) or Interplanetary Coronal Mass Ejections (ICMEs). The observed signals exhibited a periodicity due to the crossing by STEREO of the solar magnetic equator. A correlation with solar wind perturbations, and periodicities corresponding to those of Mercury and Venus were also detected (Le Chat et al. 2015). These signals nearly disappeared on STEREO A around 2012 (Le Chat et al. 2013, Malaspina et al. 2015) when the heliosphere entered a defocusing configuration in which the nanodust coming from the inner heliosphere are pushed away from the solar magnetic equator, therefore possibly preventing their observation. Observations with the RPWS instrument on board Cassini between 1 and 5 AU have produced two further important properties of interplanetary nanodust. Firstly, the average nanodust flux measured at 1 AU was similar in order of magnitude to the average of the highly variable flux measured by STEREO when the heliosphere was in a focusing configuration (Schippers et al., 2014), and decreased roughly as the inverse squared heliocentric distance (Schippers et al. 2015). Secondly, the nanodust fluxes were found to follow the variation in solar wind drift speed closely (Meyer-Vernet et al. 2017) as predicted by nanodust dynamics (Mann and Czechowski 2012).

Finally, aside from providing information on dust in the inner heliosphere, it is also quite possible that the Parker Probe and Solar Orbiter missions will find more effects that dust particles have on the solar wind. Cosmic dust particles interact with the surrounding plasma through electric charge collection, the photoelectric effect (Mann et al. 2014), and destruction processes (sputtering, fragmentation, sublimation). Photoionisation, electron-impact ionisation, and charge exchange quickly ionize the atoms and molecules in the solar wind (Mann and Czechowski, 2005) so that dust destruction generates pick-up ions. While typically near 1 AU, those interactions little affect solar wind measurable parameters (Mann et al., 2010), conditions are possibly different near the Sun. Dust particles sublimate at bulk temperatures $\approx 1000–2000$ K inside ≈ 10 solar radii (Mukai and Mukai, 1973; Mann et al., 2004; Mann and Murad, 2005). A fraction of dust material vaporizes during collision (Mann and Czechowski, 2005). The effect of dust on the solar wind is also time-variable, as for instance the dust destruction rates due to sputtering increase during coronal mass ejections (Ragot and Kahler, 2003). The solar wind particles also change charge state by interaction with the dust surface or passing through the particles (Mann et al., 2010; Minato et al., 2004). And some authors suggest that newly formed charged dust fragments generate features in the solar wind magnetic field (Connors et al., 2014; Lai et al., 2013, 2015).

7 Discussion of Implications for Observations with Parker Probe and Solar Orbiter

The design of the radio and plasma waves instrument (RPW) on the ESA Solar Orbiter (Mueller and al., 2019) is
similar to STEREO/WAVES instrumentation. The electric Antenna system (ANT) on RPW consists of a set of
three identical antennas deployed from +Z axis and from the opposite corners of the spacecraft and can operate in
dipole and monopole modes. RPW antennas consist each of a 1 metre rigid deployable boom and a 6.5 meters
stacer deployable monopole, which has a 1.5 cm radius. The Time Domain Sampler (TDS) subsystem of the RPW
instrument (Maksimovic et al., 2019) is designed to capture electromagnetic waveform snapshots at high cadence
from 200 Hz to 200 kHz, resolving in particular voltage spikes associated with interplanetary dust impacts.

Solar Orbiter will make observations of the Sun and in-situ measurements from elliptic orbits coming as close as
~60 solar radii (~0.285 AU) to the Sun. The aphelia lie outside 0.8 AU for large part of the 7 years nominal mission
time during which orbital latitude reaches 25 degree. The long cruise phase of Solar Orbiter and the elongated
spacecraft orbits with aphelia close to 1 AU provide the opportunity to study in detail the dust flux near 1AU and
to estimate the flux of sub-μm dust onto Earth, its time variation and variation during part of a solar cycle.

The FIELDS instrument on Parker Solar Probe (Bale et al. 2016) combines magnetic and electric field
measurements into a single, coordinated experiment. Four electric field antennas (2 m long, 3.18 mm diameter
Niobium C-103 thin-walled tubes) are mounted at the base of the heat shield, and deploy in full sunlight out of the
spacecraft wake, whereas a fifth antenna is mounted on the magnetometer boom in the umbra of the spacecraft.
The sensor electric field signals are transferred to a Digital Fields Board (DFB), a Time Domain Sampler (TDS)
and a Radio Frequency Spectrometer (RFS) for signal processing and digitization. The DFB and TDS make rapid
samples of waveforms with a highest sampling rate of 150,000 samples per second (DFB) and 2,000,000 samples
per second (TDS), with an on-board selection of events to reduce bit-rate. The low frequency (LF) part of the RFS
is a dual channel digital spectrometer receiving inputs from the four first antennas, either in dipole or monopole
mode, with a frequency range of 10 kHz to 2.4 MHz, allowing a relative frequency spacing of about 4.5 %.

Parker Solar Probe orbit the Sun in the ecliptic plane, making seven Venus gravity assist manoeuvres during the
seven-year nominal mission duration, which will lessen its perihelia to less than 10 R_S, the closest any spacecraft
has come to the Sun. In this way, the spacecraft will spend a total of 937 hours inside 20 R_S, 440 hours inside 15
R_S, and 14 hours inside 10 R_S (Fox et al. 2015). The surrounding plasma changes considerably along the spacecraft
orbits (Bale et al., 2016). The orbital trajectory for the first orbit around the Sun is shown in Fig. 12.

Our considerations suggest that both RPW and FIELDS measurements in monopole mode will be able to detect signals generated by dust impacts. Distinction between dust and other wave features needs to be considered based on the observational data. At present, we do not know the mass range of dust particles that will be detectable. As heliocentric distance decreases, the pulse's decay time will decrease faster than its rise time (Meyer-Vernet et al. 2017), eventually becoming smaller than the rise time, which will decrease the dust signal for large grains. The spacecraft charging and charged particles dynamics close to the Sun are expected to be considerably complicated by presence of a potential barrier (sheath structure) due to strong photoemission (Ergun et al. 2010, Campanell M. D., 2013) as well as by presence of the thermal shield and non-conducting solar panels.

Vaverka et al, (2017b) simulated pulses generated by dust impacts in various plasma environments using a simple numerical model. The spacecraft potential is calculated using orbital-motion-limited theory and the current generated by the dust impact is represented by Gaussian function. We used this approach to simulate the spacecraft charging in the inner solar system. The rise time of the pulse was estimated according to Meyer-Vernet et al. (2017) for variable photoelectron sheath. The rise time of the measured pulse is also affected by response of the antenna electronics. These electronic effects were not taken into account in the model. This model also does not describe the detailed structure of the pulses including "pre-spikes" but only their general shapes, and can be appropriate to estimate the conditions for dust impacts. Figure 13 shows estimated signals for impacts of 0.1 micrometre particles with speeds of 100 km/s for spacecraft at different distances from the Sun. The top panel represents temporal evolution of the spacecraft potential and bottom panel shows changes in the equilibrium potential. The charge production of the impact is assumed Q = 30 pC according the equation presented in chapter 2. The amplitude of the pulse is then proportional to the mass of the impinging grain and to its velocity with power between 2.5 and 6.2 (depends on materials). It is possible to see that the amplitude and duration of the pulses are reduced with decreasing distance from the sun. This fact means that the sensitivity of dust impact detection is smaller close to the sun. It is necessary to mention that the conditions for the orbital-motion-limited theory are not satisfied near the sun. The presence of the potential barrier created due to strong photoemission, described by Ergun et al. (2010) and Campanell (2013), strongly influence the spacecraft charging and charge dynamics. An interesting result is that the shape of the detected signal depends only weakly on the solar UV illumination, which leads to the photocurrent as shown in Fig. 14 for 1 AU from the sun. The increase or decrease of the solar activity which varies the UV flux, influence the spacecraft potential but not so much the profile of the pulse generated by dust impacts.

A challenge in the data analysis will be to distinguish dust impacts signals from other events. A comparison to dust measurements from other spacecraft at similar distance from the Sun as Parker Probe and Solar Orbiter should be considered. BepiColombo equipped by the Mercury Dust Monitor (MDM, Nogami et al. 2010) and electric field antennas (PWI, Kasaba et al. 2010) will in near future study the dust environment near Mercury at 0.31 to 0.47 AU from the Sun. Though also for those measurements, noise events are considered an issue, they offer an opportunity for simultaneous dust observations from several spacecraft so to have a more reliable distinction of dust impacts and other events.

Author contribution. This paper was prepared during discussions of the ISSI team on dust impacts at the International space science institute in Bern Switzerland. All authors contributed to the writing of this text in an open editing process and to the discussions that lead to the writing.

Competing interests. The authors declare that they have no conflict of interest.

Data Availability. The data will be published for open access on the UiT Open Research Repository.

Acknowledgements. This work is supported by the International Space Science Institute, ISSI in Bern in a team on Dust Impacts in spacecraft. The contributions of L. N., J. V., and J. P. were supported by Czech ministry of education youth and sport under contract LTAUSA 17066. The contributions of IM, ÅF, TA at UiT were supported by the Research Council of Norway (grant number 262941). The contribution of SY was supported by NASA through contract 1415150 with the Jet Propulsion Laboratory and CDAP grant 14397000. We thank Louis Calvinhac from University Toulouse III for preparing Fig. 12 during a student project carried out at UiT. This work was developed during several stays of some of the authors at ISSI in Bern and we wish to thank the ISSI staff for their hospitality.

References

Andersson, L., Ergun, R. E., Delory, G. T., Eriksson, A., Westfall, J., Reed, H., ... & Meyers, D. The Langmuir probe and waves (LPW) instrument for MAVEN. Space Science Reviews, 195(1-4), 173-198, 2015a.

Andersson, L., Weber, T. D., Malaspina, D., Crary, F., Ergun, R. E., Delory, G. T., ... & Andrews, D. J. Dust observations at orbital altitudes surrounding Mars. Science, 350(6261), 10.1126/science.aad0398, 2015b.

560

Andrews, D. J., Andersson, L., Delory, G. T., Ergun, R. E., Eriksson, A. I., Fowler, C. M., ... & Jakosky, B. M. Ionospheric plasma density variations observed at Mars by MAVEN/LPW. Geophysical Research Letters, 42(21), 8862-8869, 2015.

Auer, S.: Instrumentation in *Interplanetary Dust*, edited by E. Grün, pp. 385 – 444 Springer, New York, 2001

565 Bale, S. D., Goetz K., Harvey, P. R. et al.: The FIELDS Instrument Suite for Solar Probe Plus: Measuring the Coronal Plasma and Magnetic Field, Plasma Waves and Turbulence, and Radio Signatures of Solar Transients, Space Sci. Rev., 204(1-4):49-82, https://doi.org/10.1007/s11214-016-0244-5, 2016.

Belheouane, S., Zaslavsky, A., Meyer-Vernet, N., et al.: Detection of Interstellar Dust with STEREO/WAVES at 1 AU., Solar Physics, 281, 501–506, https://doi.org/10.1007/s11207-012-9995-7, 2012.

570 Burch, J., Moore, T., Torbert, R., & Giles, B., Magnetospheric multiscale overview and science objectives. Space Science Reviews, 199(1–4), 5–21, 2016.

Bougeret, J.L., Kaiser, M.L., Kellogg, P.J. et al. WAVES: The radio and plasma wave investigation on the wind spacecraft, Space Sci Rev. 71: 231. https://doi.org/10.1007/BF00751331, 1995.

575

Campanell, M. D., Negative plasma potential relative to electron-emitting surfaces, Phys. Rev. E. 88 (3), https://doi.org/10.1103/PhysRevE.88.033103, 2013.

Ceplecha, Z., Borovička, J., Elford, W.G. et al.: Meteor phenomena and bodies, Space Sci. Rev. 84 (3-4), 327–471, https://doi.org/10.1023/A:1005069928850, 1998.

580 Close, S., Linscott, I., Lee, N. et al.: Detection of electromagnetic pulses produced by hypervelocity micro particle impact plasmas, Phys. Plasmas, 20, 092102, https://doi.org/10.1063/1.4819777, 2013.

Collette, A., Grün, E., Malaspina, D., Sternovsky, Z.: Micrometeoroid impact charge yield for common spacecraft materials. J. Geophys. Res. Space Phys. 119, 6019 – 6026, https://doi.org/10.1002/2014JA020042, 2014.

Collette, A., Meyer, G., Malaspina, D., Sternovsky, Z.: impact investigation of antenna signals from dust impacts
585 on spacecraft. J. Geophys. Res. 120 (7), 5298 – 5305, https://doi.org/10.1002/2015JA021198, 2015.

Collette, A., Malaspina, D. M., Sternovsky, Z.: Characteristic temperatures of hypervelocity dust impact plasmas. J. Geophys. Res. Space Phys. 121, 2169–9402, https://doi.org/10.1002/2015JA022220, 2016.

Connors, M., Russell, C. T., Lai, H. R.: A temporary earth co-orbital linked to interplanetary field enhancements, Mon. Notices Royal Astron. Soc. 443(1), L109 –L113, https://doi.org/10.1093/mnrasl/slu092, 2014.

590 Czechowski, A., Mann, I.: Collisional vaporization of dust and production of gas in the beta Pictoris dust disk, Astrophys. J. 660(2), 1541–1555, https://doi.org/10.1086/512965, 2007.

Czechowski, A., Mann, I.: Formation and acceleration of nano dust in the inner heliosphere, Astrophys. J. 714(1), 89–99, https://doi.org/10.1088/0004-637X/714/1/89, 2010.

Czechowski, A., Mann, I. in: (I. Mann, N. Meyer-Vernet, A. Czechowski Eds.) Nanodust in the Solar System:
595 Discoveries and Interpretations, Astrophysics and Space Science Library 385, 47–75, Springer, New York, 2012.

Dietzel, H., et al. The HEOS 2 and HELIOS micrometeoroid experiments. Journal of Physics E: Scientific Instruments 6.3:209, doi: 10.1088/0022-3735/6/3/008, 1973.

Drapatz, S and Michel, K. W.: Theory of shock-wave ionization upon high-velocity impact of micrometeorites. Zeitschrift für Naturforschung A, 29.6: 870-879, https://doi.org/10.1515/zna-1974-0606, 1974.

600 Ergun, R. E., Malaspina, D. M., Bale, S. D., McFadden, J. P., Larson, D. E., Mozer, F. S., Meyer-Vernet, N., Maksimovic, M., Kellogg, P. J., Wygant, J. R.: Spacecraft charging and ion wake formation in the near-Sun environment, Phys. Plasmas 17, 072903, https://doi.org/10.1063/1.3457484, 2010.

Fox, N. J. et al. The Solar Probe Plus mission: humanity's first visit to our star, Space Sci. Rev. 2015, DOI 10.1007/s11214-015-0211-6

605 Gurnett, D. A., R. L. Huff, and D. L. Kirchner, The wide-band plasma wave investigation, Space Sci. Rev., 79(1–2), 195–208, 1997.

Gurnett, D., Ansher, J. A., Kurth, W. S., Granroth, L. J.: Micron-sized dust particles detected in the outer solar system by the Voyager 1 and 2 plasma wave instruments, Geophys. Res. Lett. 24 (24), 3125–3128, https://doi.org/10.1029/97GL03228, 1997.

610 Gurnett, D. A.: Principles of Space Plasma Wave Instrument Design, Measurement Techniques for Space Plasmas, AGU Monograph 103, ed. by R. Pfaff, J. Borovsky, and D. Young, American Geophysical Union, Washington, DC, 121–136, 1998.

Gurnett, D. A., Kurth, W. S., Kirchner, D. L., Hospodarsky, G. B., Averkamp, T. F., Zarka, P., Lecacheux, A., Manning, R., Roux, A., Canu, P., Cornilleau-Wehrlin, N., Galopeau, P., Meyer, A., Bostrom, R., Gustafsson, G., Wahlund, J. –E., Aahlen, L., Rucker, H. O., Ladreiter, H. –P., Macher, W., Woolliscroft, L. J. C., Alleyne, H., Kaiser, M. L., Desch, M. D., Farrell, W. M., Harvey, C. C., Louarn, P., Kellogg, P. J., Goetz, K. and Pedersen, A.: The Cassini radio and plasma wave science investigation, Space Sci. Rev., 114(1-4), 395–463, https://doi.org/10.1007/s11214-004-1434-0, 2004.

Gustafsson, G., et al. First results of electric field and density observations by Cluster EFW based on initial months of operation, Ann. Geophys., 19(10), 1219–1240, 2001.

Grün, E., Pailer, N., Fechtig, H., & Kissel, J. (1980). Orbital and physical characteristics of micrometeoroids in the inner solar system as observed by Helios 1. Planetary and Space Science, 28(3), 333–349. http://doi.org/10.1016/0032-0633(80)90022-7

Grün, E., Zook, H. A., Fechtig, H., Giese, R. H.: Collisional balance of the meteoritic complex, Icarus 62 (2), 244–272, https://doi.org/10.1016/0019-1035(85)90121-6, 1985.

Grün, E., Gustafson, B., Mann, I., et al.: Interstellar dust in the heliosphere, Astron. Astrophys. 286(3), 915–924, 1994.

Grün, E., Srama, R., Krüger, H., et al.: 2002 Kuiper prize lecture: Dust astronomy, Icarus, 174(1), 1–14, https://doi.org/10.1016/j.icarus.2004.09.010, 2005.

Göller, J. R., & Grün, E. Calibration of the Galileo/Ulysses dust detectors with different projectile materials and at varying impact angles. Planetary and Space Science, 37(10), 1197-1206, https://doi.org/10.1016/0032-0633(89)90014-7, 1989.

Havnes, O., Trøim, J., Blix, T., et al.: First detection of charged dust particles in the Earth's mesosphere, J. Geophys. Res. Space Phys. 101(A5), 10839-10848, doi: 10.1029/96JA00003, 1996.

Hornung, K., & Kissel, J.: On shock wave impact ionization of dust particles. Astronomy and Astrophysics, 291, 324-336. 1994.

Ishimoto, H., Mann, I.: Modeling the particle mass distribution within 1 AU of the Sun, Planet. Space Sci. 47 (1-2), 225-232, https://doi.org/10.1016/S0032-0633(98)00083-X, 1999.

Jakosky, B. M., Lin, R. P., Grebowsky, J. M., Luhmann, J. G., Mitchell, D. F., Beutelschies, G., ... & Baker, D. The Mars atmosphere and volatile evolution (MAVEN) mission. Space Science Reviews, 195(1-4), 3-48, 2015.

John, W., Reischl, G., & Devor, W.: Charge transfer to metal surfaces from bouncing aerosol particles. Journal of Aerosol Science, *11*(2), 115-138, https://doi.org/10.1016/0021-8502(80)90029-4 1980.

645 Jones, A.P., Tielens, A.G.G.M, Hollenbach, D.J., Grain shattering in shocks: the interstellar grain size distribution, Astrophys. J. 469, 740-764, 1996.

Jones, G.H., Balogh, A., McComas, D. J., MacDowall, R.J.: Strong Interplanetary Field Enhancements at Ulysses-Evidence of dust trails' interaction with the solar wind? , Icarus 166 (2), 297-310, https://doi.org/10.1016/j.icarus.2003.09.007, 2003.

650 Jones, G.H., Knight, M.M., Battams, K., et al.:The Science of Sungrazers, Sunskirters, and Other Near-Sun Comets, Space Sci. Rev. 214:20. 2018.

Juhasz, A., Horanyi, M.: Dynamics and distribution of nano-dust particles in the inner solar system, Geophys. Res. Lett. 40 (11), 2500-2504, https://doi.org/10.1002/grl.50535, 2013.

Kasaba Y., Bougeret J.-L., Blomberg L.G., Kojima H., Yagitani S., … & Matsumoto H. The Plasma Wave
655 Investigation (PWI) onboard the BepiColombo/ MMO: First measurement of electric fields, electromagnetic waves, and radio waves around Mercury. Planetary and Space Science, 58, 238–278, 2010.

Kimura, H. Ishimoto, H., Mukai, T.: A study on solar dust ring formation based on fractal dust models, Astron. Astrophys, 326(1), 263-270, 1997.

Kellogg, P. J., Goetz, K., & Monson, S. J. Dust impact signals on the wind spacecraft. Journal of Geophysical
660 Research: Space Physics, 121(2), 966-991, 10.1002/2015JA021124, 2016.

Kurth, W. S., Averkamp, T. F., Gurnett, D. A., and Wang, Z.: Cassini RPWS observations of dust in Saturn's E ring, Planet. Space Sci., 54 (9-10), 988-998, https://doi.org/10.1016/j.pss.2006.05.011, 2006.

Lai, H. R., Wei, H. Y., and Russell, C. T.: Solar Wind Plasma Profiles During Interplanetary Field Enhancements (IFEs): Consistent with Charged-Dust Pickup, SOLAR WIND 13: AIP CP 1539, 402-405,
665 https://doi.org/10.1063/1.4811070, 2013.

Lai, H. R., Russell, C. T., Jia, Y. D., Wei, H. Y., and Angelopoulos, V.: Momentum transfer from solarwind to interplanetary field enhancements inferred from magnetic field draping signatures, Geophys. Res. Lett. 42(6), 1640-1645, https://doi.org/10.1002/2015GL063302, 2015.

670 Lebreton, J., van Lieshout, R., Augereau, J.-C. et al.: An interferometric study of the Fomalhaut inner debris disk III. Detailed models of the exozodiacal disk and its origin, Astron. Astrophys. 555, A146 (20 pp), https://doi.org/10.1051/0004-6361/201321415, 2013.

Le Chat, G., Zaslavsky, A., Meyer-Vernet, N., Issautier, K., et al.: Effect of the Interplanetary Medium on Nanodust Observations by the Solar Terrestrial Relations Observatory, Solar Phys. 286, 549-559, 2013.

Le Chat, G., Issautier, K., Zaslavsky, A., et al.: Interplanetary nanodust detection by the Solar Terrestrial Relations

675 Observatory/WAVES low frequency receiver, Solar Phys. 290 (3), 933-942, https://doi.org/10.1007/s11207-015-0651-x, 2015.

Levasseur-Regourd, A.C., Mann, I., Dumont, R., Hanner, M.S., in: (E. Grün, B.A.S. Gustafson, S. Dermott, H. Fechtig Eds.) Interplanetary Dust, Astronomy and Astrophysics Library, 57- 94 (Springer, Heidelberg), 2001.

MacQueen, R.M.: Infrared observations of outer solar corona, Astrophys. J. 154(3P1), 1059-, doi: 10.1086/149825,

680 1968.

Maksimovic, M. et al., The Radio and Plasma Waves (RPW) instrument on the Solar Orbiter Mission, Astron. & Astrophys., submitted, 2019.

Mann, I.: The solar F-corona-Calculations of the optical and infrared brightness of circumsolar dust, Astron. Astrophys, 261(1), 329-335, 1992.

685 Mann, I.: Interstellar dust in the solar system, Ann. Rev. Astron. Astrophys. 48, 173–203, https://doi.org/10.1146/annurev-astro-081309-130846, 2010.

Mann, I., Czechowski, A.: Dust destruction and ion formation in the inner solar system, Astrophys. J. 621(1), L73-L76, https://doi.org/10.1086/429129, 2005.

Mann, I., Murad, E.: On the existence of silicon nanodust near the Sun, Astrophys. J. 624(2), L125-L128,

690 https://doi.org/10.1086/430701, 2005.

Mann, I., Kimura, H., Biesecker, D.A., et al.: Dust near the Sun, Space Sci. Rev. 110(3-4), 269-305, doi:10.1023/B:SPAC.0000023440.82735.ba., 2004.

Mann, I., Murad, E., Czechowski, A.: Nanoparticles in the inner solar system, Planet. Space Sci. 55(9), 1000-1009, https://doi.org/10.1016/j.pss.2006.11.015 , 2007.

695 Mann, I. Pellinen–Wannberg, A., Murad, E. et al.: Dusty Plasma Effects in Near Earth Space and Interplanetary Medium, Space Sci. Rev. 161(1-4), 1-47, https://doi.org/10.1007/s11214-011-9762-3, 2011.

Mann, I., Czechowski, A., Meyer-Vernet, N.: Dust in the interplanetary medium – interactions with the solar wind, Solar Wind 12, AIP CP 1216, 491-496, https://doi.org/10.1063/1.3395911, 2010.

Mann, I., Meyer–Vernet, N., Czechowski, A.: Dust in the planetary system: Dust interactions in space plasmas of 700 the solar system, Physics Reports 536(1), 1–39, https://doi.org/10.1016/j.physrep.2013.11.001, 2014.

Malaspina, D. M., Horanyi, M., Zaslavsky, A., et al.: Interplanetary and interstellar dust observed by the Wind WAVES electric field instrument, Geophys. Res. Lett, 41(2):266–272, https://doi.org/10.1002/2013GL058786, 2014.

Malaspina, D. M., O'Brien, L. E., Thayer, F., Sternovsky, Z., & Collette, A. Revisiting STEREO interplanetary and 705 interstellar dust flux and mass estimates. Journal of Geophysical Research: Space Physics, 120(8), 6085-6100, 10.1002/2015JA021352, 2015.

Malaspina, D. M., and Wilson, L. B. A database of interplanetary and interstellar dust detected by the Wind spacecraft. Journal of Geophysical Research: Space Physics, 121(10), 9369-9377. 10.1002/2016JA023209, 2016

710

McBride, N., and J. A. M. McDonnell, Meteoroid impacts on spacecraft: Sporadics, streams, and the 1999 Leonids, Planet. Space Sci., 47(8–9), 1005–1013, https://doi.org/10.1016/S0032-0633(99)00023-9, 1999.

McCrea, I., Aikio, A., Alfonsi, L., et al.: The science case for the EISCAT_3D radar, Prog. Earth Planet. Sci. 2, 21, https://doi.org/10.1186/s40645-015-0051-8, 2015.

715 McDonnell, J. A. M., Gardner, D. J.: Meteoroid morphology and densities: Decoding satellite impact data, Icarus 133 (1), 25–35, https://doi.org/10.1006/icar.1998.5912, 1998.

Meyer-Vernet, N.: Comet Giacobini-Zinner diagnosis from radio measurements, Adv. Space Res. 5(12), 1985.
Meyer-Vernet, N., Lecacheux, A., Pedersen, B.: Constraints on Saturn's E ring from Voyager 1 radio astronomy instrument, Icarus, 123(1), 113-128, https://doi.org/10.1006/icar.1996.0145 , 1996.

720 Meyer-Vernet, N.: Detecting dust with electric sensors in planetary rings, comets and interplanetary space, ESA SP-476, 635–639, 2001.

Meyer-Vernet, N., Lecacheux, A., Kaiser, M. L., Gurnett, D. A.: Detecting nanoparticles at the radio frequencies: Jovian dust stream impacts on Cassini/RPWS, Geophys. Res. Lett., 36(3), 3103,1-5 https://doi.org/10.1029/2008GL036752, 2009.

725 Meyer-Vernet, N., Maksimovic, M., Czechowski, A. et al.: Dust Detection by the Wave Instrument on STEREO: Nanoparticles Picked up by the Solar Wind, Solar Physics, 256(1-2), 463-474, https://doi.org/10.1007/s11207-009-9349-2, 2009.

Meyer-Vernet, N. Zaslavsky, A. in: I. Mann, N. Meyer-Vernet, A. Czechowski (Eds.), Nanodust in the Solar System: Discoveries and Interpretations, Springer, Heidelberg, 133–160, 2012.

730 Meyer-Vernet, N., Moncuquet, M., Issautier, K., Lecacheux, A.: The importance of monopole antennas for dust observations: why Wind/WAVES does not detect nanodust, Geophys. Res. Lett., 41(8), 2716-2720, https://doi.org/10.1002/2014GL059988, 2014.

Meyer-Vernet, N., Mann, I., Le Chat, G. et al.: The physics and detection of nanodust in the solar system, Plasma Phys. Control. Fusion, 57(1), 014015, https://doi.org/10.1088/0741-3335/57/1/014015, 2015.

735 Meyer-Vernet, N., Moncuquet, M., Issautier, K., Schippers, P.: Frequency range of dust detection in space with radio and plasma wave receivers: theory and application to interplanetary nanodust impacts on Cassini, J. Geophys. Res. 121, https://doi.org/10.1002/2016JA023081, 2017.

Minato, T., Köhler, M., Kimura, H., Mann, I., Yamamoto, T.: Momentum transfer to interplanetary dust from the 740 solar wind, Astron. Astrophys. 424(2), L13-L16, https://doi.org/10.1051/0004-6361:200400037, 2004.

Miyachi, T., Fujii, M., Hasebe, N., Miyajima, M., Okudaira, O., Takechi, S., Onishi, T., Minami, S., Shibata, H., Ohashi, H. and Iwai, T.. Measurement of temperature after hypervelocity collision of microparticles in the range from 10 to 40 km/s. Applied Physics Letters, 93(17), p.174107, 2008.

745

Mocker A., Bugiel S., Auer S., Baust G., Colette A., Drake K., … & Srama R., A 2 MV Van de Graaff accelerator as a tool for planetary and impact physics research. Rev. Sci. Instrum. 82, 095111, https://doi.org/10.1063/1.3637461, 2011.

750

Mukai, T., Mukai, S.: Temperature and motion of grains in interplanetary space, Publ. Astronom. Soc. Japan, 25(4), 481-488, 1973.

Mukai, T., Yamamoto, T.: Model of the circumsolar dust, Publ. Astronom. Soc. Japan, 31(3), 585-596, 1979.

Mueller, M. et al., The SOlar Orbiter Mission, Astron. Astrophys., submitted, 2019.

755 Němeček, Z., Pavlů, J.,Šafránková, J., et al.: Lunar Dust Grain Charging by Electron Impact: Dependence of the Surface Potential on the Grain Size, Astrophys. J., 738(1): Art. No. 14 (7 pages), https://doi.org/10.1088/0004-637X/738/1/14, 2011.

Nesvorný, D.; Janches, D.; Vokrouhlický, D.; Pokorny, P.; Bottke, W. F.; Jenniskens, P. Astrophys. J. 2011, 743, 129.

760 Nogami, K. Fujiib, M. Ohashi, H., et al. Development of the Mercury dust monitor (MDM) onboard the BepiColombo mission Planetary and Space Science 58 (2010) 108–115

Nouzák, L., Hsu, S., Malaspina, D., Thayer, F. M., Ye, S. Y., Pavlů, J., et al.: Laboratory modeling of dust impact detection by the Cassini spacecraft, Planetary and Space Science, 156, 85–91, http://doi.org/10.1016/j.pss.2017.11.014, 2018.

765 Ohgaito, R., Mann, I., Kuhn, J.R., MacQueen, R.M., Kimura, H.: The J- and K-band brightness of the solar F corona observed during the solar eclipse on 1998 February 26, Astrophys. J., 578(1), 610-620, http://doi.org/10.1086/342426, 2002.

Pantellini, F., Belheouane, S., Meyer-Vernet, N., Zaslavsky, A.: Nano dust impacts on spacecraft and boom antenna charging, Astrophys. Space Sci., 341(2), 309-314, doi:10.1007/s10509-012-1108-4, 2012.

770 Pellinen-Wannberg, A., Kero, J., Häggström, I., Mann, I., Tjulin, A.: The forthcoming EISCAT_3D as an extra-terrestrial matter monitor, Planet. Space Science, 123, 33-40, http://dx.doi.org/10.1016/j.pss.2015.10.009, 2016.

Plane, J. M. C.: Cosmic dust in the earth's atmosphere, Chem. Soc. Rev., 41(19), 6507-6518, https://doi.org/10.1039/c2cs35132c, 2012.

Ragot, B. R., Kahler, S. W.: Interactions of dust grains with coronal mass ejections and solar cycle variations of 775 the F-coronal brightness, Astrophys. J., 594(2), 1049-1059, https://doi.org/10.1086/377076, 2003.

Russell, C. T., Luhmann, J., Barnes, A., Mihalov, J. D., Elphic, R. C.: An unusual interplanetary event - encounter with a comet, Nature, 305 (5935), 612-615, https://doi.org/10.1038/305612a0, 1983.

Sánchez-Lavega, A., Muñoz, A. G., Garcia-Melendo, E., Perez-Hoyos, S., Gomez-Forrellad, J. M., Pellier, C., ... & Parker, D. An extremely high-altitude plume seen at Mars' morning terminator. Nature, 518(7540), 525. 10.1038/nature14162, 2015.

Schippers, P., Meyer-Vernet, N., Lecacheux, A., Kurth, W. S., Mitchell, D. G., André, N.: Nanodust detection near 1 AU from spectral analysis of Cassini/Radio and Plasma Wave Science data. Geophys. Res. Lett. 41, 5382-5388, https://doi.org/10.1002/2014GL060566, 2014.

Schippers, P., Meyer-Vernet, N., Lecacheux, A., Belheouane, S., Moncuquet, M., Kurth, W. S., Mann, I.: Nanodust detection between 1 and 5 AU using Cassini wave measurements, Astrophys. J., 806(77), https://doi.org/10.1088/0004-637X/806/1/77, 2015.

Schultz, P. H., Sugita, S., Eberhardy, C. A., & Ernst, C. M. The role of ricochet impacts on impact vaporization. International journal of impact engineering, *33*(1-12), 771-780, https://doi.org/10.1016/j.ijimpeng.2006.09.005, 2006.

Shu, A., Collette, A., Drake, K., Grün, E., Horanyi, M., Kempf, S., Mocker, A., Munsat, T., Northway, P., Srama, R., Sternovsky, Z., Thomas, E.: 3 MV hypervelocity dust accelerator at the Colorado center for lunar dust and atmospheric studies. Rev. Sci. Instrum., 83 (7), 5108, https://doi.org/10.1063/1.4732820, 2012.

Sittler, E.C., Thomsen, M., Johnson, R. E., Hartle, R. E., Burger, M., Chornay, D., Shappirio, M.D., Simpson, D., Smith, H. T., Coates, A. J. and Rymer, A.M.: Cassini observations of Saturn's inner plasmasphere: Saturn orbit insertion results, Planetary and Space Science, 54(12), 1197-1210, https://doi.org/10.1016/j.pss.2006.05.038, 2006.

Srama, R., Ahrens, T. J., Altobelli, N., Auer, S., Bradley, J. G., Burton, M., ... & Grande, M. The Cassini cosmic dust analyzer. In The Cassini-Huygens Mission (pp. 465-518). Springer, Dordrecht., 10.1007/978-1-4020-2774-1_7, 2004.

Stauffer, J. R., Stenborg, G., & Howard, R. A. Measuring the Flattening of the Outer F-corona Using STEREO-A/HI-1 Images. The Astrophysical Journal, 864(1), 29, 10.3847/1538-4357/aad689, 2018.

805   Stenborg, G., & Howard, R. A., A Heuristic Approach to Remove the Background Intensity on White-light Solar Images. I. STEREO/HI-1 Heliospheric Images, Astrophysical Journal, 839, 68, 10.3847/1538-4357/aa6a12, 2017a.

Stenborg, G., & Howard, R. A., The Evolution of the Surface of Symmetry of the Interplanetary Dust from 24° to 5° Elongation, Astrophysical Journal, 848, 57, 10.3847/1538-4357/aa8ef0, 2017b.

810

Stenborg, G., Howard, R. A., & Stauffer, J. R., Characterization of the White-light Brightness of the F-corona between 5° and 24° Elongation, Astrophysical Journal, 862, 168, 10.3847/1538-4357/aacea3, 2018.

Thayer, F. M., D. M. Malaspina, A. Collette, and Z. Sternovsky, Variation in relative dust impact charge

815   recollection with antenna to spacecraft potential on STEREO, J. Geophys. Res. Space Physics, 121, 4998–5004, https://doi.org/10.1002/2015JA021983, 2016.

Torbert, R. B., Russell, C. T., Magnes, W., et al., The FIELDS instrument suite on MMS: Scientific objectives, measurements, and data products. Space Science Reviews, 199(1–4), 105–135, 2016.

820

Tsintikidis, D., Gurnett, D. A., Granroth, L. J., Allendorf, S. C., Kurth, W. S.: A revised analysis of micron-sized particle detected near Saturn by the Voyager 2 plasma wave instrument, J. Geophys. Res., 99(A2), 2261, https://doi.org/10.1029/93JA02906, 1994.

825   Vaverka, J., Pellinen-Wannberg, A., Kero, J., Mann, I., De Spiegeleer, A., Hamrin, M., Norberg, C., Pitkänen, T.: Detection of meteoroid hypervelocity impacts on the Cluster spacecraft: First results, J. Geophys. Res. Space Phys. 122(6), 6485–6494, https://doi.org/10.1002/2016JA023755, 2017a.

Vaverka, J., Pellinen-Wannberg, A., Kero, J; Mann, I., De Spiegeleer, A., Hamrin, M., Norberg, C., Pitkänen, T.: Potential of Earth Orbiting Spacecraft Influenced by Meteoroid Hypervelocity Impacts, IEEE Trans. Plasma Sci.,

830   45(8), 2048–2055, https://doi.org/10.1109/TPS.2017.2676984, 2017b.

Vaverka, J., Nakamura, T., Kero, J., Mann, I., De Spiegeleer, A., Hamrin, M., Norberg, C., Lindqvist, P-A., Pellinen-Wannberg, A.: Comparison of Dust Impact and Solitary Wave Signatures Detected by Multiple Electric Field Antennas Onboard the MMS Spacecraft, J. Geophys. Res. Space Phys., 123(8), 6119–6129, https://doi.org/10.1029/2018JA025380, 2018.

835   Wahlund, J. E., Boström, R., Gustafsson, G., Gurnett, D. A., Kurth, W. S., Averkamp, T., Hospodarsky, G. B., Persoon, A. M., Canu, P., Pedersen, A., Desch, M. D.: The inner magnetosphere of Saturn: Cassini RPWS cold plasma results from the first encounter. Geophys. Res. Lett., 32(20), https://doi.org/10.1029/2005GL022699, 2005.

Wehry, A., Mann, I.: Identification of beta-meteoroids from measurements of the dust detector onboard the Ulysses spacecraft, Astron. Astrophys. 341(1), 296-303, 1999.

840   Wood, S. R., Malaspina, D. M., Andersson, L., & Horanyi, M.. Hypervelocity dust impacts on the Wind spacecraft: Correlations between Ulysses and Wind interstellar dust detections. Journal of Geophysical Research: Space Physics, 120(9), 7121-7129, 10.1002/2015JA021463, 2015.

Ye, S.Y., Gurnett, D.A., Kurth, W.S., Averkamp, T.F., Morooka, M., Sakai, S. and Wahlund, J.E., 2014. Electron
845   density inside Enceladus plume inferred from plasma oscillations excited by dust impacts. Journal of Geophysical Research: Space Physics, 119(5), pp.3373-3380. https://doi.org/10.1002/2014JA019861

Ye, S. -Y., Gurnett, D. A., Kurth, W. S., Averkamp, T. F., Kempf, S., Hsu, H. W., Srama, R., Grün, E.: Properties of dust particles near Saturn inferred from voltage pulses induced by dust impacts on Cassini spacecraft, J. Geophys. Res. Space Phys., 119(8), https://doi.org/10.1002/2014ja020024, 2014.

850   Ye, S.Y., Gurnett, D.A. and Kurth, W.S., 2016. In-situ measurements of Saturn's dusty rings based on dust impact signals detected by Cassini RPWS. Icarus, 279, pp.51-61. https://doi.org/10.1016/j.icarus.2016.05.006

Ye, S.-Y., Kurth, W. S., Hospodarsky, G. B., Averkamp, T. F., Gurnett, D. A.: Dust detection in space using the monopole and dipole electric field antennas, J. Geophys. Res. Space Phys.,121(12),11964-11972, https://doi.org/10.1002/2016JA023266, 2016.

855   Ye, S. -Y., W. S. Kurth, G. B. Hospodarsky, A. M. Persoon, D. A. Gurnett, M. Morooka, J. -E. Wahlund, H. -W. Hsu, M. Seiss, R. Srama, Cassini RPWS dust observation near Janus and Epimetheus orbits, JGR, https://doi.org/10.1029/2017JA025112, 2018.

Ye, S.Y., Kurth, W.S., Hospodarsky, G.B., Persoon, A.M., Sulaiman, A.H., Gurnett, D.A., Morooka, M., Wahlund,
860   J.E., Hsu, H.W., Sternovsky, Z. and Wang, X., 2018. Dust Observations by the Radio and Plasma Wave Science Instrument During Cassini's Grand Finale. Geophysical Research Letters, 45(19), pp.10-101.

Ye S., Vaverka J., Nouzak L., Sternovsky Z., Zaslavsky A., … & Horanyi M., Understanding Cassini RPWS Antenna Signals Triggered by Dust Impacts (supporting information), Geophys. Res. Lett., https://doi.org/10.1029/2019GL084150, 2019.

865   Zaslavsky, A., Meyer-Vernet, N., Mann, I., et al.: Interplanetary dust detection by radio antennas: Mass calibration and fluxes measured by STEREO/WAVES, J. Geophys. Res., 117(A5), A05102, https://doi.org/10.1029/2011JA017480, 2012.

Zaslavsky, A.: Floating potential perturbations due to micrometeoroid impacts: Theory and application to S/WAVES data, J. Geophys. Res., 120(2), 855-867, https://doi.org/10.1002/2014JA020635, 2015.

870

Dust Cloud Near Sun
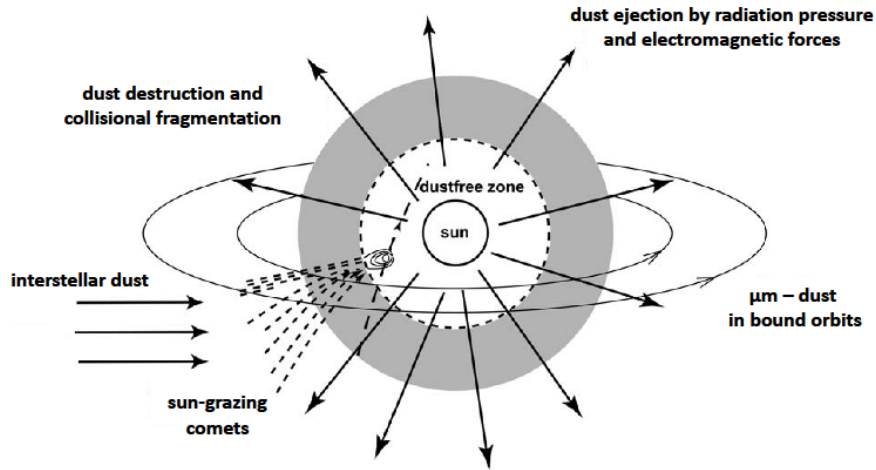
Figure 1: Sketch of different dust components and dust interactions in the vicinity from the Sun as given in an overview (adapted from Mann et al., 2014). Recent results are presented in section 6.
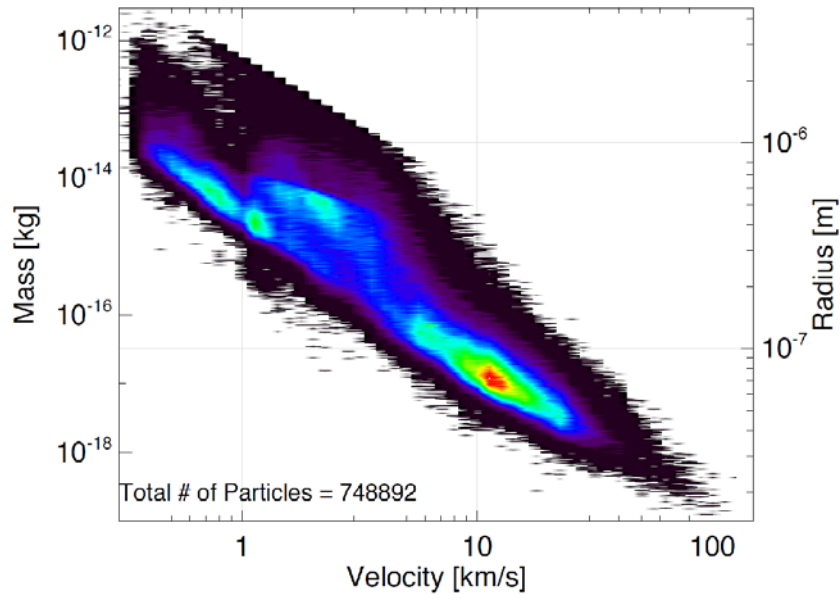
Figure 2: The mass vs. velocity distribution of iron dust particles generated by the accelerator facility at the University of Colorado.
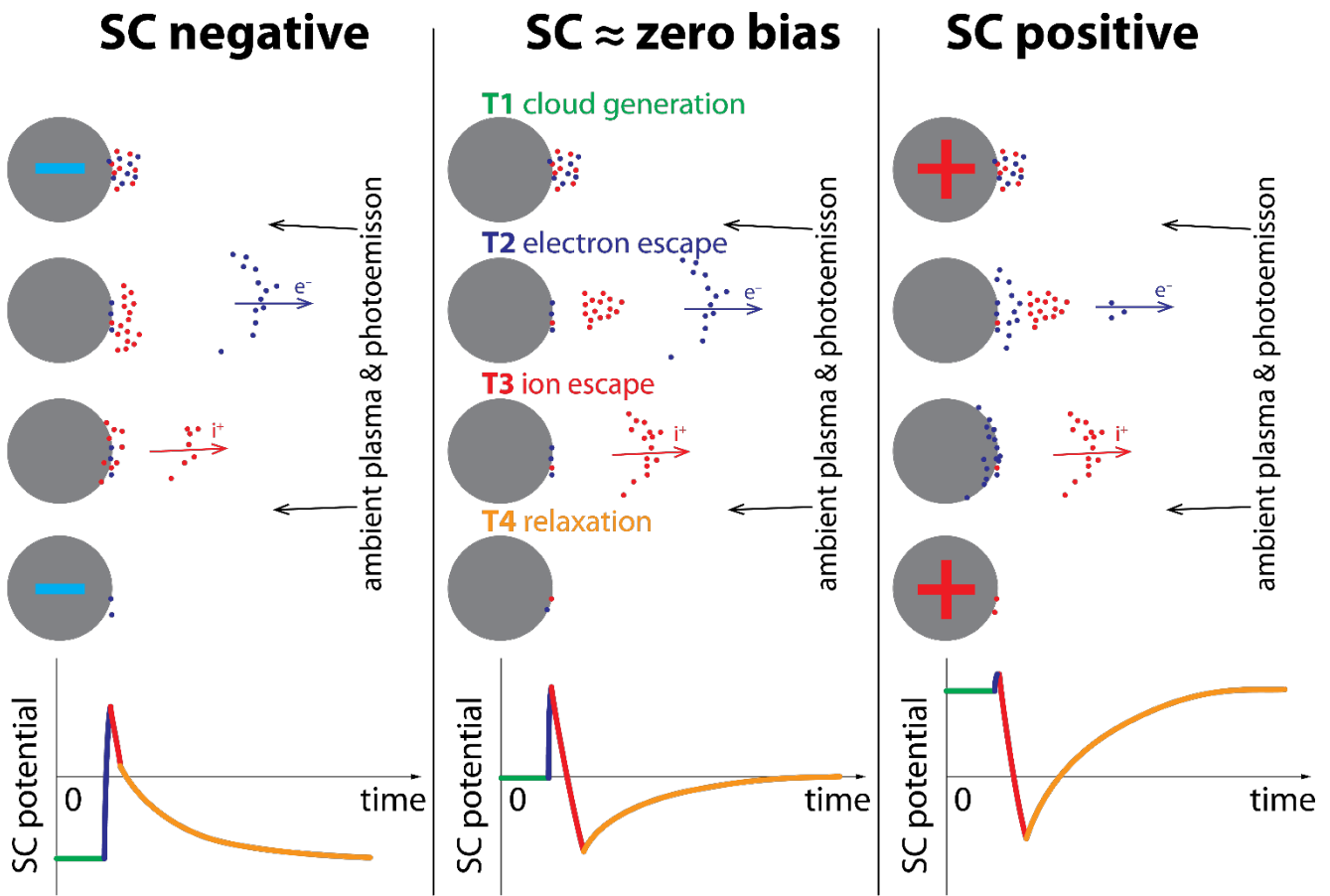
880

Figure 3: This figure sketches the impact process for a spacecraft that is slightly negatively charged (left panel), zero biased (middle panel), and slightly positively charged (right panel). It is further described in the text and parameters given in Table 1.
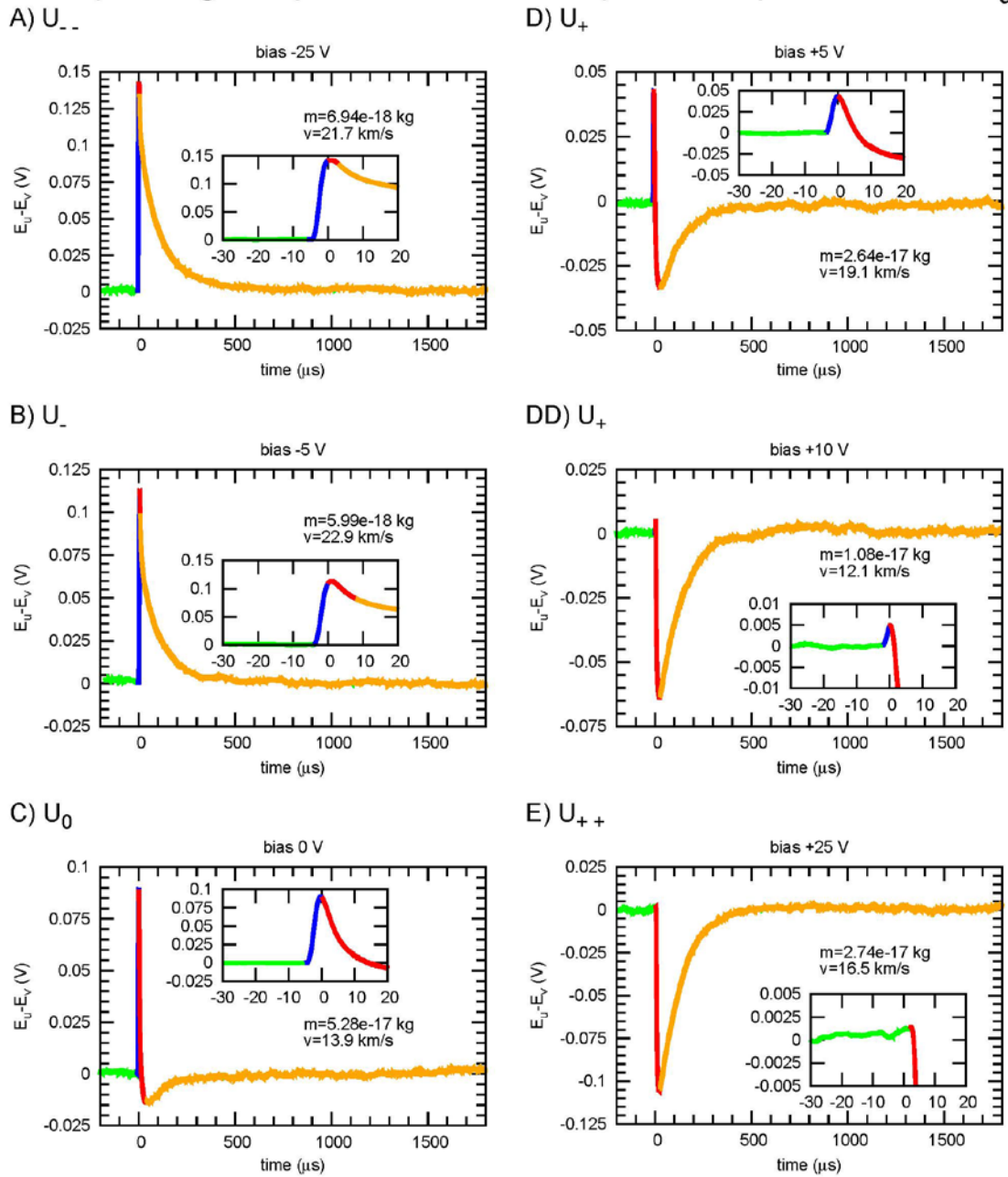
Figure 4: Laboratory simulation of dust impacts on Cassini model showing the impact signal detected by the antenna (E$_U$ boom was bombarded) for different polarity and size of bias voltage. Different phases of dust impact signal are distinguished by colours (green – cloud generation, blue – electron escape, red – ion escape, orange – relaxation). The inserts show details of the pre-spikes (modified from Nouzák et al., 2018). The conditions in these laboratory measurements are comparable to a measurement in monopole configuration on the spacecraft.
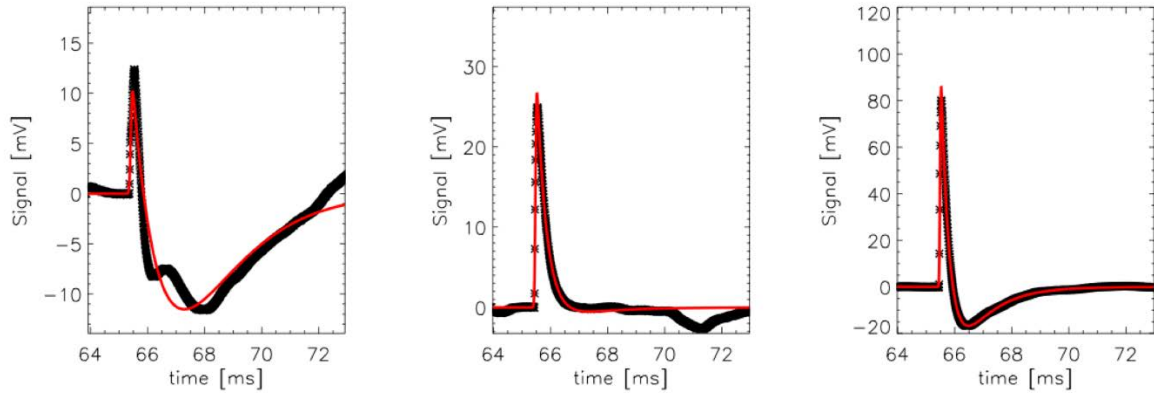
Figure 5: Dust impact signals recorded by the STEREO/WAVES TDS on STEREO A shown with black crosses show in comparison to fit with semi-empirical model shown with red solid lines (from Zaslavsky et al. 2015).
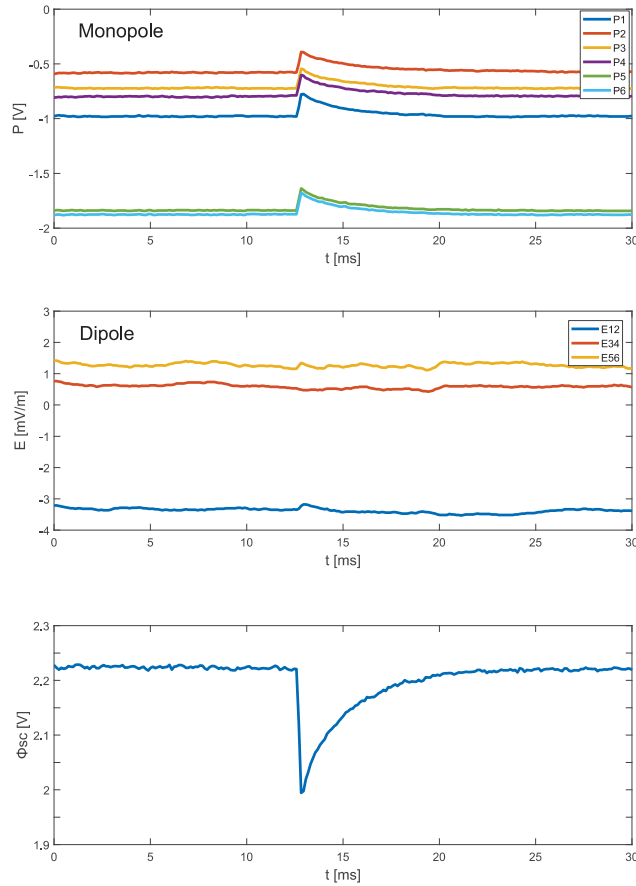
Figure 6: A potential signal of dust impact measured with MMS. Example of a typical event related to the change of the spacecraft potential observed in monopole configuration (upper panel), the dipole measurements (middle panel) with a lack of signal and the derived voltage pulse in the lower panel (cf. Vaverka et al. 2018).
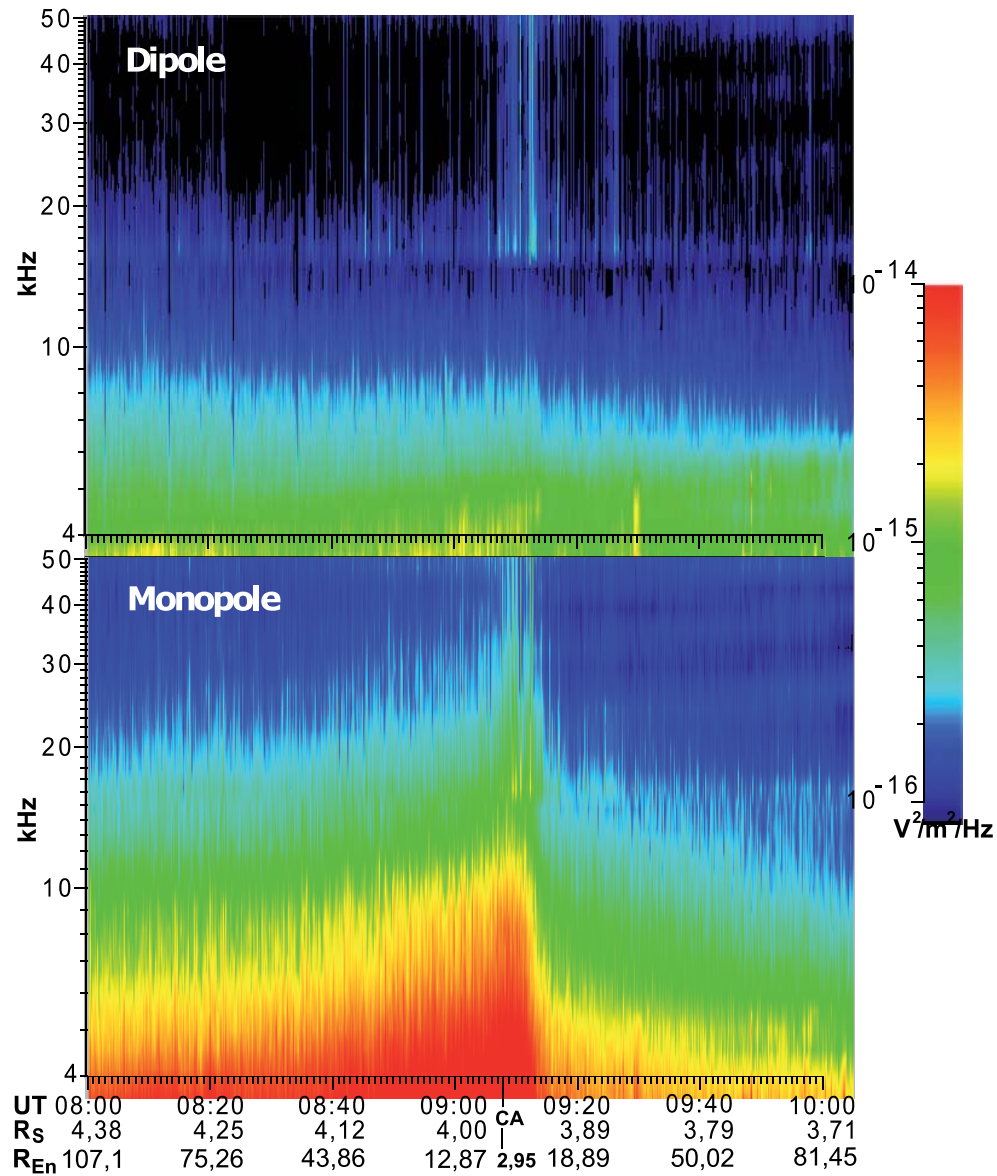
Figure 7: From Meyer-Vernet et al. (2014): Time-frequency electric power spectral density measured by Cassini/ RPWS on 9 March 2005 in Saturn's E ring, in dipole (top) and monopole mode (bottom). The increase due to micron-sized dust impacts on the spacecraft only appears in monopole mode, whereas the dipole only measures the weaker plasma quasi-thermal and impact noise.

905
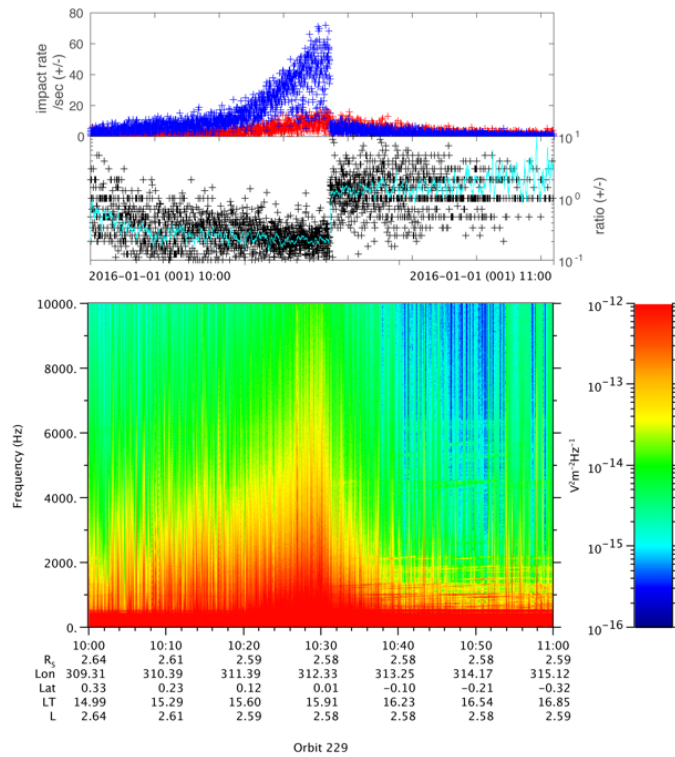
Figure 8: Adapted from Fig. 4 and 5 of Ye et al. 2016b. RPWS wave power spectrogram around a ring plane crossing on DOY 001, 2016. The top panel shows the positive (red) and negative (blue) impact rates. The middle panel shows the impact signal polarity ratios with the moving averages (teal). At ~10:30, the antenna used was switched from monopole to dipole, which was accompanied by a decrease in the spectral power and the polarity ratio jumping back to 1.
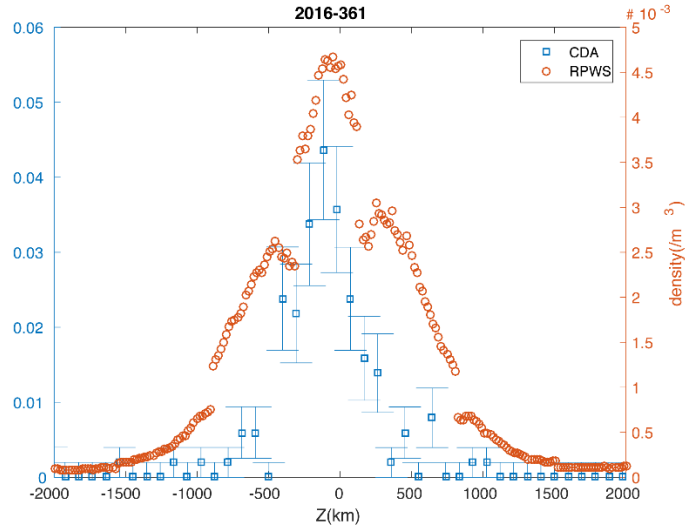
Figure 9: Adapted from Fig. 4 of Ye et al. 2018a. Comparison of vertical dust density profiles of the Janus-Epimetheus ring measured by RPWS and CDA during the ring plane crossing on DOY 361, 2016. There is one order of magnitude difference between the two results, which is within the uncertainty limit estimated for the RPWS measurement (Ye et al. 2014).
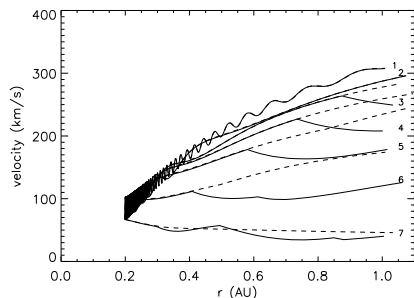
Figure 10: Velocity as function of distance from the Sun for particles with Q/m = 10^{-4}, 10^{-5}, 10^{-6}, and 10^{-7} e/m$_p$ released from a circular orbit with the radius 0.2 AU near the ecliptic. Solid lines correspond to the focusing, and dashed to defocusing, magnetic field orientation (adapted from Mann et al., 2014).

920
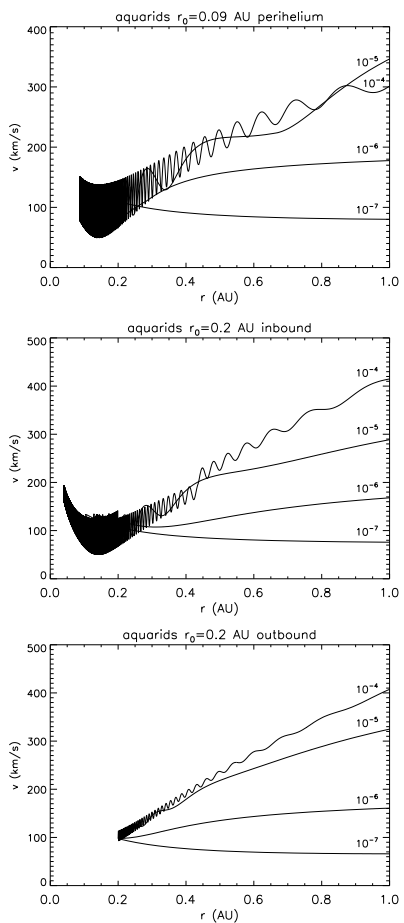
Figure 11: Velocities of small fragments released from Aquarid meteoroids as function of the heliocentric distance. The velocities are calculated for dust with Q/m = 10^{-4}, 10^{-5}, 10^{-6} and 10^{-7} e/m$_p$. The ratio of surface charge to mass corresponds to sizes 3 nm, 10 nm, and larger. The particles are released from the orbit of Aquarids at the perihelion (0.09 AU from the Sun, the upper panel), and at the distance 0.2 AU on the inbound (middle panel) and outbound (lower panel) parts of the orbit. From (Czechowski and Mann,
925 **2018)**
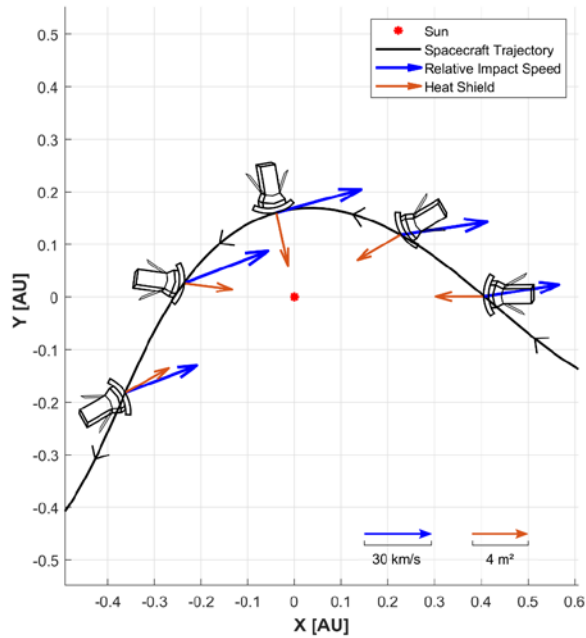
Figure 12: Parker Solar Probe trajectory during first perihelion passage. Blue arrows indicate speed of spacecraft relative to the dust particles in circular orbit. Red arrows indicate surface vector of the spacecraft heatshield (Figure courtesy of L. Calvinhac).

930
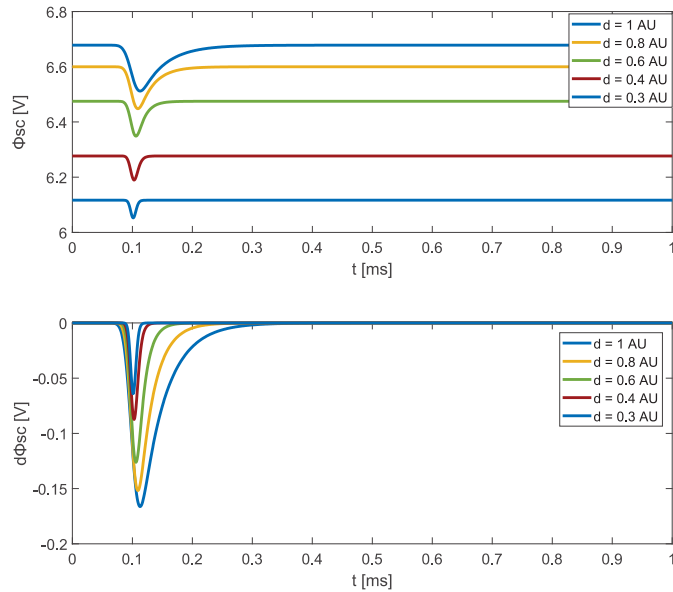
Figure 13: The estimated signals for impacts of 0.1 micrometre particles with speed 100 km/s for spacecraft at different distance from the Sun. The charge production of the impact is assumed Q = 30 pC. Estimate based on Vaverka et al. (2017b) model.
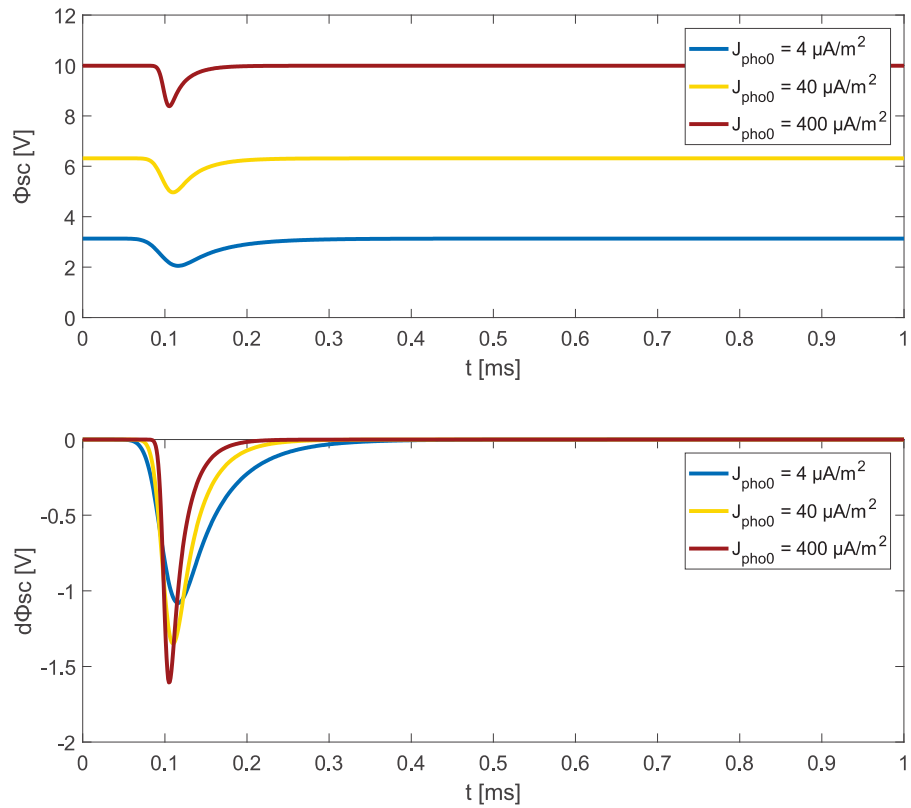
935 **Figure 14: The spacecraft potential change during dust impact for different values of the photocurrent. A typical value of photocurrent at 1 AU is 40 µA/m². While its influence on spacecraft potential is considerable, this is not for the change induced by impacts.**

940

Table 1: Explanation of impact process signal shape illustrated in Fig. 3.

	T1) cloud gen.	T2) electron escape	T3) ion escape	T4) relaxation
Negative spacecraft potential ($U_{sc,0} < 0$)	Cloud generation and expansion ($U_{sc,0} < 0$)	Electron escape ($U_{sc,T2} > U_{sc,0} < 0$)	Ion escape suppressed ($U_{sc,T3} < U_{sc,T2}$)	Relaxation ($U_{sc,T4} => U_{sc,0}$)
Spacecraft potential zero ($U_{sc,0} \sim 0$)	Cloud generation and expansion ($U_{sc,0} = 0$)	Partial electron escape ($U_{sc,T2} > U_{sc,0} = 0$)	Partial ion escape ($U_{sc,T3} < U_{sc,T2}$)	Relaxation ($U_{sc,T4} => U_{sc,0}$)
Positive spacecraft potential ($U_{sc,0} > 0$)	Cloud generation and expansion ($U_{sc,0} > 0$)	Electron escape suppressed ($U_{sc,T2} > U_{sc,0} > 0$)	Ion escape ($U_{sc,T3} < U_{sc,T2}$)	Relaxation ($U_{sc,T4} => U_{sc,0}$)

945 **Table 2: Examples of signal development for different bias (spacecraft potential) shown in Fig. 4.**

	A)	B)	C)	D) and DD)	E)
Process and current (positive is toward spacecraft)	U negative U_{--}	U slightly negative U_{-}	U zero U_0	U slightly positive U_{+}	U positive U_{++}
Electron recollection	zero	suppressed	partial	enhanced	full
Ion recollection	full	enhanced	partial	suppressed	zero
Electron escape	full — fast	enhanced	partial — fast	suppressed	zero
Ion escape	close to zero	suppressed	partial — slow	enhanced	full — slow
Relaxation	full	reduced	close to zero	reduced	full